DIAMOND DISSOLUTION IN Na_2CO_3, Na_2CO_3-NaCl, AND Na_2CO_3-NaF MELTS AT 950°C AND 0.1 MPa

Erin Keltie

Submitted in Partial Fulfillment of the Requirements
for the Degree of Bachelor of Sciences, Honours
Department of Earth Sciences
Dalhousie University, Halifax, Nova Scotia
April 28, 2016

Distribution License

DalSpace requires agreement to this non-exclusive distribution license before your item can appear on DalSpace.

NON-EXCLUSIVE DISTRIBUTION LICENSE

You (the author(s) or copyright owner) grant to Dalhousie University the non-exclusive right to reproduce and distribute your submission worldwide in any medium.

You agree that Dalhousie University may, without changing the content, reformat the submission for the purpose of preservation.

You also agree that Dalhousie University may keep more than one copy of this submission for purposes of security, back-up and preservation.

You agree that the submission is your original work, and that you have the right to grant the rights contained in this license. You also agree that your submission does not, to the best of your knowledge, infringe upon anyone's copyright.

If the submission contains material for which you do not hold copyright, you agree that you have obtained the unrestricted permission of the copyright owner to grant Dalhousie University the rights required by this license, and that such third-party owned material is clearly identified and acknowledged within the text or content of the submission.

If the submission is based upon work that has been sponsored or supported by an agency or organization other than Dalhousie University, you assert that you have fulfilled any right of review or other obligations required by such contract or agreement.

Dalhousie University will clearly identify your name(s) as the author(s) or owner(s) of the submission, and will not make any alteration to the content of the files that you have submitted.

If you have questions regarding this license please contact the repository manager at dalspace@dal.ca.

Grant the distribution license by signing and dating below.

_____ _____

Name of signatory Date

ABSTRACT

Kimberlites are the source of most natural diamonds, and despite extensive study many aspects of such magmas remain enigmatic. Their explosive method of emplacement indicates high volatile content, but the composition of these volatiles is still poorly constrained. Kimberlitic diamonds often show resorption features such as rounded morphologies and trigonal etch pits which develop from interaction between the diamond surface and fluids in the kimberlite melt. Experimental studies at high pressures have reproduced many resorption features of natural diamonds and indicated the effect of the composition of kimberlitic fluid on diamond resorption morphology. However, the extent and character of diamond resorption in a kimberlite body after the emplacement is not known. This study exposed unresorbed kimberlitic diamonds to melts of Na_2CO_3, Na_2CO_3-NaCl, and Na_2CO_3-NaF at 950ºC and 0.1 MPa. The developed resorption features were measured using atomic force microscopy (AFM). The study examines how the presence of halogens in the carbonate melt affects diamond dissolution kinetics and the morphology of positively oriented trigonal etch pits. The study confirmed that positive trigons can be produced by near-surface resorption. Comparison of the experimentally produced positive trigons to those present on natural diamonds from Snap Lake kimberlite allows us to shed more light on the process of emplacement of the Snap Lake dyke. Results of this study provide new insights into the mechanism of diamond resorption as well as the occurrence and evolution of etch pits on the diamond surface by observing how the same trigons change from consequent runs with AFM.

Key words: kimberlite fluid composition, diamond dissolution, carbonate-halogen melts, AFM, experimental petrology

TABLE OF CONTENTS

LIST OF FIGURES

LIST OF TABLES

ACKNOWLEDGEMENTS

AFM work was supported by the NSERC grant to Yana Fedortchouk. Diamonds from Yakutia were provided by Dr. A Logvinova. I thank Yana Fedortchouk for her guidance and exceptional availability during this project, Zhuoyuan Li for his help using the AFM, and Ryan Kressall for his thoughtful discussion on kimberlites. I would also like to thank Danielle Stanton-Turcotte for her patient explanations of chemistry concepts, and my parents Richard and Sheila Keltie for their never ending support.

CHAPTER 1: INTRODUCTION

1.1 Kimberlites and diamonds

1.1.1 General background

Kimberlites are an enigmatic rock type that is the source of the majority of the world's natural diamonds, and thus are of economic interest. Kimberlites are volatile-rich ultrabasic igneous rocks with mantle-sourced xenoliths and megacrysts set in a fine-grained matrix (Mitchell, 1986) that generally occur as cone or carrot-shaped intrusions, often called pipes, in continental regions underlain by cratons. The widely accepted model of kimberlitic melt is one that is Mg-rich, ultrabasic, hydrous, and enriched in incompatible trace elements (Kamenetsky et al, 2009). Although such a melt composition is consistent with the observed kimberlite mineralogy, it is inconsistent with other kimberlite properties such as inferred magma temperatures, rheological properties, and style of magma ascent and emplacement (Kamenetsky et al, 2009).

Kimberlites occur in regions of continental crust that are underlain by cratons that usually have an older (>2.4 Ga) core and an attached belt of younger (>1.0 Ga) deformed rocks. Kimberlites that contain diamonds usually occur in regions where the craton core is older than 2.4 Ga (Mitchell, 1986). The craton is commonly overlain by sedimentary or volcanic rocks of Phanerozoic age. These areas of the crust where kimberlite magmatism occurs are called kimberlite provinces (Mitchell, 1986). Kimberlite provinces in Southern Africa, the Northwest Territories of Canada, and Siberia have the most economically valuable diamond mines. Figure 1.1.1 shows areas of Earth with cratons and associated kimberlites.

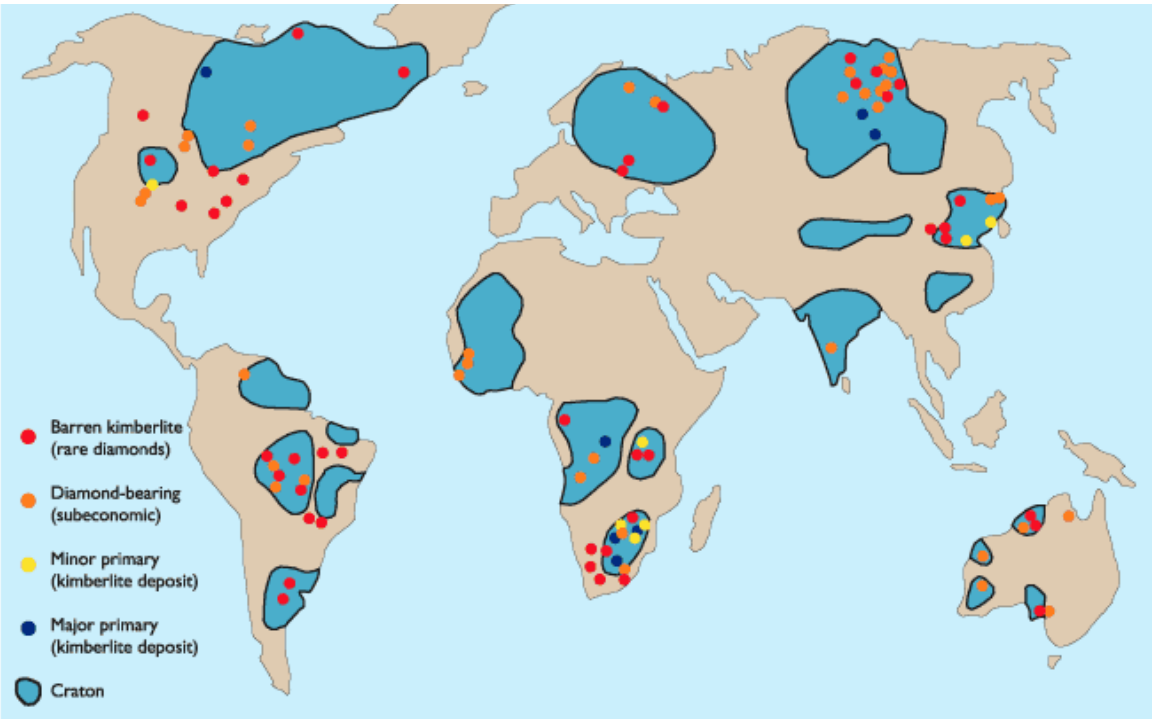

Figure 1.1.1. Global craton and kimberlite distribution. Areas of cratonized crust are outlined and shaded. Kimberlites are represented by circles. Kimberlite occurrence is correlated with areas of cratonized crust; those that exist outside of cratons are usually not diamondiferous. Eckstrand et al. (1995).

Kimberlitic diamonds often show various resorption features that indicate their dissolution in the kimberlite magma as well as during residence in the mantle (Fedortchouk, 2015). The morphology of diamond resorption features depends on the composition and conditions of diamond-destructive fluids in both environments (Fedortchouk, 2015) and can be used as a mineralogical tool to provide more information about kimberlitic fluids and the emplacement process.

1.1.2 Volatiles in kimberlites

Kimberlite magmas are believed to have a very high volatile content, evidenced by their explosive method of emplacement, as well as measured values as high as 15 wt% CO_2 and 12 wt% H_2O (Brooker et al, 2011). Although the origin of these volatiles is still unclear, the presence of primary calcite and phlogopite in kimberlites shows significant

magmatic concentration of both CO_2 and H_2O in kimberlite magma (Brooker et al, 2011). High carbonate content indicates that kimberlitic magma is CO_2-rich (Mitchell, 1986). Experimental studies on diamond resorption (Fedortchouk et al, 2010) and geochemical data from a global kimberlite geochemistry database (Kjarsgaard et al, 2009) indicate that kimberlitic magma is also H_2O-rich. The diamondiferous Udachnaya-East kimberlite pipe in Siberia, a rare example of an unaltered kimberlite, has anomalous mineralogy which allowed Kamenetsky et al. (2009) to propose a chlorine-rich composition for kimberlite magma. Hydrous minerals are rare in the Udachnaya-East pipe, which contains up to 6 wt% chlorine, with abundant halides in the groundmass of the deepest and freshest exposures (Kamenetsky et al, 2009). Kamenetsky et al. (2009) suggest that the primary magmatic characteristics of the Udachnaya-East kimberlite were low H_2O contents as well as high Cl and Na contents, and that in general, a melt composition rich in CO_2 and Cl may be an alternative to the widely-accepted H_2O- and CO_2-rich model of kimberlitic melt (Kamenetsky et al, 2009).

Diamond resorption features have been proposed to be a proxy for kimberlitic fluid composition (Fedortchouk, 2015; Zhang et al, 2015), however the effect of halogens on the morphology of diamond resorption features is poorly understood (Sonin et al, 2009). It is also not well known how much resorption happens after kimberlite emplacement at the surface. While the experimental data on diamond resorption at near surface conditions (0.1 MPa) is very limited, the existing studies show development of positively-oriented trigonal etch pits at low pressure (Fedortchouk and Canil, 2009). These positive trigons are extremely rare on natural diamonds, with the exception of those occurring on diamonds from the Snap Lake kimberlite (Li et al, 2015).

1.2 Objectives of this study

This study aims to shed light on multiple questions regarding diamond dissolution features and how they may relate to kimberlitic fluids and emplacement. Exposure of kimberlitic diamonds to melts of Na_2CO_3, Na_2CO_3-NaCl, and Na_2CO_3-NaF at 950ºC and atmospheric pressure (0.1 MPa) and mapping the resulting features using atomic force microscopy (AFM) will allow us to test if positively-oriented trigonal etch pits are a product of near-surface resorption and to examine the character of resorption that would occur after kimberlite emplacement. This study also examines how the presence of halogens in the carbonate melt affects diamond dissolution kinetics and the morphology of dissolution features. Observing how the same trigons develop as a function of time may provide new insights into the mechanism of diamond resorption and the evolution of etch pits on the diamond surface. Finally, comparison of experimentally produced trigons with natural trigons on diamonds from the Snap Lake kimberlite in the Northwest Territories allows us to shed light on the conditions of diamond resorption and the kimberlite emplacement process.

CHAPTER 2: BACKGROUND

2.1 Resorption morphology on diamond

2.1.1 Classification of diamond morphology and resorption features

Diamonds have different morphologies that reflect their growth conditions. Although there are multiple ways to classify diamond morphologies, the most generalized schemes tend to best emphasize different growth mechanisms. Orlov (1973) classified diamonds into ten groups (I-X) based on their colour, morphology and crystal habit.

Diamonds in groups I-V are all monocrystalline and are divided based on octahedral or cubic morphology as well as colour and presence of a coating (Orlov, 1973). Diamonds in groups VI-X are aggregrate diamonds further divided based on colour (Orlov, 1973). Sunagawa (1984) classified diamonds into three groups based on their growth conditions: monocrystalline growth, polycrystalline growth, and single crystal transitioning into polycrystalline growth. These morphologies are summarized in Figure 2.1.1.

Monocrystalline diamonds grow as individual crystals when the growth rate is slow. They occur as octahedrons, cubes, or rhombic dodecahedrons (Tappert and Tappert, 2011). Octahedral diamonds are most common, although often their eight faces are not perfectly equal in area due to one growth direction being more favourable than another (Tappert and Tappert, 2011). Some monocrystalline diamonds have a cubic habit with rough faces that are often curved and rounded edges (Tappert and Tappert, 2011). Diamonds may switch between these two growth patterns during crystallization, but often one pattern is dominant as true cubo-octahedral diamonds are rarely found (Tappert and Tappert, 2011). Dodecahedral habits are caused by resorption of octahedral or cubic diamonds, which occurs when they are entrained in kimberlitic magma bringing them to

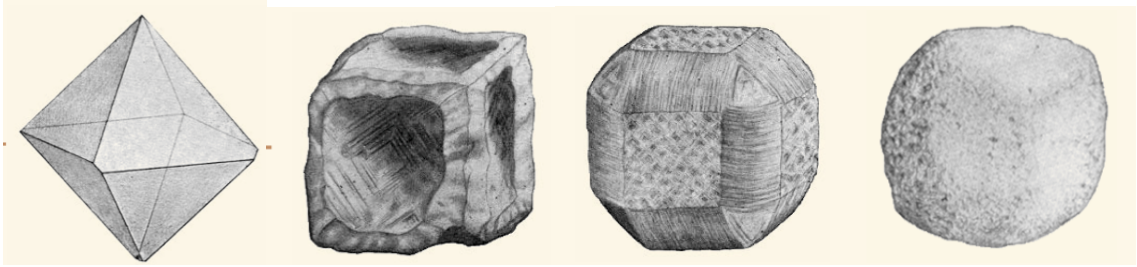

Figure 2.1.1. Diamond morphologies and classification. From left to right: monocrystalline octahedral, monocrystalline cubic, cubic with fibrous coat, and polycrystalline. Tappert and Tappert (2011).

the surface (Tappert and Tappert, 2011). Monocrystalline diamonds can also exhibit parallel intergrowths, twinning, or exist as aggregates of a small number of crystals (Tappert and Tappert, 2011). If a diamond does not have an identifiable crystal habit, it is called irregular. They usually have smooth, undulating faces and occur frequently. Diamonds may also be fragmented after crystallization in the mantle, transportation to the surface, or in the mining process (Tappert and Tappert, 2011).

Fibrous diamonds are interpreted to have a faster rate of growth than monocrystalline diamonds (Tappert and Tappert, 2011). Fibrous diamonds have microscopic parallel fibers that are oriented in the same direction as crystal growth. The fibers contain many microscopic inclusions, which cause the diamond to look translucent or opaque (Tappert and Tappert, 2011). Fibrous diamonds often form cubic habits with the characteristic rough faces and rounded edges, but they can also be irregular. Occasionally, fibrous coats will surround an inner monocrystalline diamond (Tappert and Tappert, 2011). The inner diamond, being protected from resorption, is often a well-defined octahedron. The habit of the monocrystalline diamond underneath heavily influences the shape of fibrous coated diamonds (Tappert and Tappert, 2011).

Polycrystalline diamonds are interpreted have the fastest rate of growth and are aggregates of many microcrystalline or cryptocrystalline diamond crystals. The individual crystals are interlocking and the overall aggregate lacks any crystal habit (Tappert and Tappert, 2011). When a polycrystalline diamond is comprised of euhedral crystals surrounded by smaller grains, it is called a framesite (Tappert and Tappert, 2011). Several kimberlite deposits contain framesite diamonds (Tappert and Tappert, 2011). Other examples of polycrystalline diamonds include carbonados and yakutites.

Carbonados have smaller grain sizes, higher porosity, and a darker colour than framesites due to the presence of other minerals such as florencite, xenotime, zircon, native metals, and alloys lining pore spaces (Tappert and Tappert, 2011). Yakutites, named for their discovery in Yakutia, Russia, contain a hexagonal polymorph of diamond called lonsdaleite (Tappert and Tappert, 2011).

The conditions that diamonds are exposed to at different stages in their history produce many types of surface features. Some features develop while the diamond is in the Earth's mantle, while others develop during transport in kimberlite magma or at the Earth's surface. An understanding of the textural relationships to diamond history can help refine models of kimberlite emplacement.

Diamonds undergo growth, plastic deformation, and resorption while in the Earth's mantle (Tappert and Tappert, 2011). During growth, diamonds may develop triangular growth plates that form stepped surfaces on octahedral diamonds (Fig. 2.1.2a). When diamonds are grown synthetically, conditions that favour rapid nucleation result in faces with imbricated triangular growth plates (Wentorf, 1965). Another feature diamonds develop in the mantle are shield-shaped laminae, layers that are smaller than the face below with curved edges (Tappert and Tappert, 2011). They are generally thinner than triangular growth plates (Robinson, 1979) and form due to resorption of growth layers (Robinson, 1979; Tappert and Tappert, 2011).

One of the most widely observed surface features on natural diamonds are trigonal pits, commonly referred to as trigons (Robinson, 1979). They are commonly oriented opposite to the face on which they occur, in which case they are referred to as

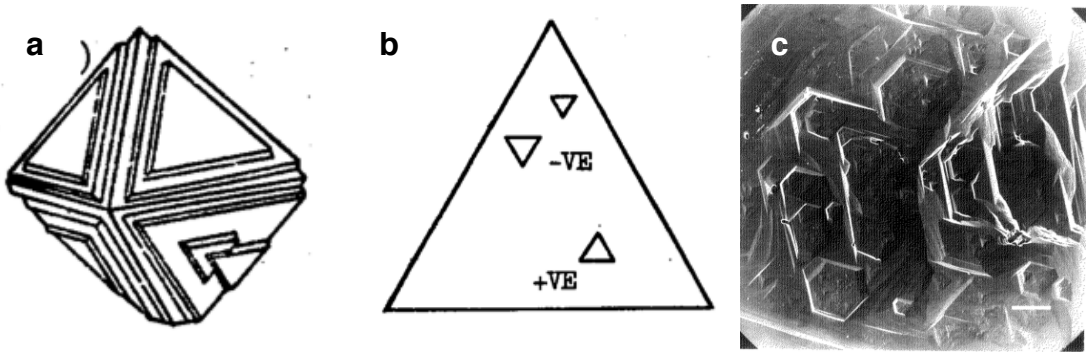

Figure 2.1.2. Diamond growth and resorption features. (a) Sketch of triangular growth plates. (b) Sketch of negative and positive trigons. (c) Hexagonal etch pits. The scale bar in the lower right corner represents 0.1 mm. Robinson (1979).

negative trigons, shown in Figure 2.1.2b (Tappert and Tappert, 2011). Positive oriented trigons are rarely observed on natural diamonds (Tappert and Tappert, 2011). Trigons may have pointed, flat, or terraced bottoms. The size and depth of trigons varies greatly, even within the same diamond face (Tappert and Tappert, 2011). Trigons are a result of resorption, in which dissolution occurs at defect sites on the diamond surface (Robinson, 1979). Some pits are not triangular but rather hexagonal (Figure 2.1.2c) or tetragonal (Tappert and Tappert, 2011). Tetragonal pits form on cubic diamond faces and are usually terraced and negatively oriented (Tappert and Tappert, 2011). Hexagonal pits are not well understood and are thought to be the product of interactions between the etching effects of oxygen and carbon dioxide (Robinson, 1979). They are usually flat-bottomed and occasionally contain trigons within them (Robinson 1979).

2.1.2 Studies of natural kimberlitic diamonds

The morphology and resorption features on diamonds from kimberlites in the Northwest Territories of Canada have been extensively studied. Gurney et al. (2004) described diamonds from two groups of kimberlites from the Ekati property of the Northwest territories and found that diamond characteristics varied greatly between

kimberlites as well within an individual kimberlite pipe. Octahedral and dodecahedral morphologies were common, with subordinate cubic morphologies with fibrous coats present as well (Gurney et al, 2004). Diamond colour was predominantly colourless, brown, or yellow and diamond faces were flat or stepped (Gurney et al, 2004). Some diamonds featured negative trigons (Gurney et al, 2004). Gurney et al. (2004) divided diamonds into four broad groups, octahedral, cubic, cubo-octahedral, and dodecahedral, based on crystal habit and then further divided each group into subgroups based on colour and surface features. Each subgroup was referred to as a "building block", and Gurney et al. (2004) proposed using "building blocks" to explain the sources of difference diamond populations within kimberlites.

Fedortchouk et al. (2010) used diamonds from several kimberlite pipes in the Ekati property, to compare their resorption features to those produced experimentally in the presence of H_2O or CO_2 fluid aiming to examine possible effect of the composition of kimberlitic fluid on diamond population. Octahedral morphologies were present in each kimberlite, while hexoctahedral morphologies were also present in varying degrees in some kimberlites (Fedortchouk et al, 2010). Some octahedral diamonds were unresorbed, possibly having been protected from resorption processes by being encased in a xenolith (Fedortchouk et al, 2010). Most octahedral diamonds featured dissolution features such as trigonal pits, hexagonal pits, circular disks, striations, and pointed corners in various proportions and combinations (Fedortchouk et al, 2010). Some hexoctahedral diamonds had no surface features, while others featured dissolution features such as striations, hillocks, deformation lamellae, and trigons in various proportions and combinations (Fedortchouk et al, 2010). Experimental results suggested that the differences in

resorption morphologies of diamonds from different pipes were due to the loss of fluids during the emplacement of some of the kimberlites (Fedortchouk et al, 2010). Fluid loss during emplacement affects diamond resorption by causing sharp, irregular dissolution features to develop, as well as slowing down the emplacement of magma and allowing diamonds to be exposed to kimberlitic melt at high temperatures for a longer amount of time (Fedortchouk et al, 2010).

Zhang and Fedortchouk (2012) further examined the morphology and resorption features on diamonds from the same kimberlites in the Northwest Territories, focusing on the types of resorption morphologies produced during diamond partial dissolution in the mantle. They grouped diamonds into four broad groups: unresorbed, kimberlite-induced resorption, mantle-derived resorption, and undefined features. Unresorbed diamonds were flat faced with no resorption features and also represent one of the mantle-derived categories. Diamonds with kimberlite-induced resorption have ditrigonal [111] faces and were split into three groups based on the fluid present during the resorption (Zhang and Fedortchouk, 2012). H_2O-rich fluids produced smooth faces, large shallow trigons, striations, and circular disks; CO_2-rich fluids produced small point-bottomed trigons or shallow hexagons; and fluid-poor environments produced frosted faces with sharp pointed features (Zhang and Fedortchouk, 2012). Diamonds in the mantle-derived resorption category had trigonal [111] faces and were split into two main groups based on the complexity of their features (Zhang and Fedortchouk, 2012): complex morphologies and stepped-face morphologies. Complex features included deep hexagonal and trigonal pits with stepped walls, or highly dense trigonal pits (Zhang and Fedortchouk, 2012). Diamonds with stepped faces combine a large range of morphologies including trigonal

steps, beveled trigonal steps, irregular layers with straight or edges and sharp corners, irregular layers with curved edges and rounded corners, or irregular trigon-bearing layers at different heights (Zhang and Fedortchouk, 2012). Undefined diamonds either did not have [111] faces or had irregular [111] faces (Zhang and Fedortchouk, 2012). Zhang and Fedortchouk (2012) then compared diamond morphologies to their internal properties and found that diamonds with the same morphological style have similar nitrogen contents and follow the same isotherm. This indicates that morphological style is a reflection of mantle history (Zhang and Fedortchouk, 2012).

2.1.3 Experimental studies

Experimental studies of diamond dissolution started as early as the 1960s. The earliest experimental studies of diamond dissolution mostly focused on the kinetics of diamond dissolution and the effect of H_2O and CO_2 on diamond oxidation rate (Rudenko et al, 1967). Many of these studies were conducted at conditions far from those of natural kimberlitic diamonds.

Khokhryakov and Pal'yanov (2001) used experimental data to describe the general morphological evolution of diamond during dissolution. For octahedral diamonds, edges become progressively rounder until the [111] face is completely truncated, forming an octahedroid, and further dissolution rounds the diamond further into a "Ural-type" dodecahedroid (Khokhryakov and Pal'yanov, 2001; Khokhryakov and Pal'yanov, 2007). Pseudorhombic dodecahedral diamonds also eventually evolve into "Ural-type" dodecahedroids, while cubic diamonds evolve into tetrahexahedroids (Khokhryakov and Pal'yanov, 2001; Khokhryakov and Pal'yanov, 2007). Khokhryakov

and Pal'yanov (2002) showed that morphological characteristics such as etch pits and striation patterns serve as an indicator for redox conditions during the dissolution process by running dissolution experiments at 5.7 GPa and 1400ºC with varying oxygen fugacities. In highly oxidizing conditions diamonds developed curvifaced trisoctahedral shapes and positive trigons, in moderately oxidizing conditions diamonds developed negative trigons, and in reducing conditions diamonds developed flat-faced trisoctahedral shapes and negative trigons (Khokhryakov and Pal'yanov, 2002).

Kozai and Arima (2005) investigated the dissolution rate and morphological progression of diamonds when exposed to kimberlitic melt at 1 GPa and 1300ºC–1420ºC in the graphite stability field. They found that as experimental runs progressed, no surface graphitization was observed and the diamonds changed from octahedrons with flat [111] faces to nearly spherical tetrahexahedroids with undetectable [111] faces over the course of 360 minutes (Kozai and Arima, 2005). Intermediate forms of octahedrons with rounded edges and combinations of octahedrons and tetrahexahedroids with shrinking [111] faces were observed as the run progressed (Kozai and Arima, 2005). Negatively oriented trigons developed on the [111] faces that began as dense, shallow trigons and progressed to few, large trigons (Kozai and Arima, 2005). Morphological changes were accompanied with a decrease in the weight of the diamonds, indicating that the diamonds underwent dissolution in the kimberlitic melt in the graphite stability field and that dissolution is a combination of volume resorption and surface etching (Kozai and Arima, 2005). At 1300ºC, the dissolution rate was 0.0017–0.12 mm/hr depending on the buffer used (Kozai and Arima, 2005). At 1420ºC, the dissolution rate was 0.014 mm/hr (Kozai and Arima, 2005). They found that in general, increasing the temperature,

and oxygen fugacity increases diamond dissolution rate (Kozai and Arima, 2005). The amount of time a diamond could survive dissolution in a melt is highly dependent upon the redox conditions in the melt, with more oxidizing conditions greatly increasing the rate of dissolution (Kozai and Arima, 2005). They also found that using a carbonate solvent suppressed dissolution (Kozai and Arima, 2005; Kozai and Arima, 2008).

Fedortchouk et al. (2007) studied diamond dissolution in two synthetic compositions of natural aphanitic Jericho kimberlite, natural alkali basalt, and synthetic simple-system kimberlite (volatile-free with H_2O added) and found that free fluid must be present in the melt in order to develop resorption features that are similar to those commonly present on natural diamonds, as diamonds develop surface graphitization and/or irregular cavities when volatiles are absent or below their saturation limit in the melt. They also found that at 1150ºC–1350ºC and 1 GPa their dissolution rates in H_2O fluid and in CO_2 fluid agreed well with those from Kozai and Arima (2005) in natural kimberlite, indicating that dissolution processes that occur in pure fluid are the same that occur in melt-fluid systems and must represent dissolution processes in natural kimberlites (Fedortchouk et al, 2007). In H_2O fluids, crystal edges were rounded quickly, striations developed on tetreahexahedral faces, and a few large, flat-bottomed negative trigons developed on [111] faces (Fedortchouk et al, 2007). In CO_2 fluids, crystal edges were preserved at larger diamond weight loss, hillocks developed on the tetrahexahedral faces, and numerous small point-bottomed trigons developed, most of which were negative but including some positive-oriented trigons as well (Fedortchouk et al, 2007). These findings show that in HCO fluid, surface features are predicable from the fluid composition (Fedortchouk et al, 2007).

Khokhryakov and Pal'yanov (2010) ran diamond dissolution experiments at 5.7-7.4 GPa and 1400-1750ºC with dry carbonate melts, carbonate melt with CO_2, and carbonate melt with H_2O. They found that changes in melt composition affect the dissolution features that form. In dry melts, diamonds developed positive point-bottomed trigons; in melts with CO_2, diamonds developed positive flat- and point-bottomed trigons; in melts with H_2O, diamonds developed negative flat-bottomed trigons (Khokhryakov and Pal'yanov, 2010). Based on their results, Khokhryakov and Pal'yanov (2010) proposed morphological evolution schemes for octahedral diamonds in dry, CO_2-bearing, and H_2O-bearing carbonate melts (Figure 2.1.3).

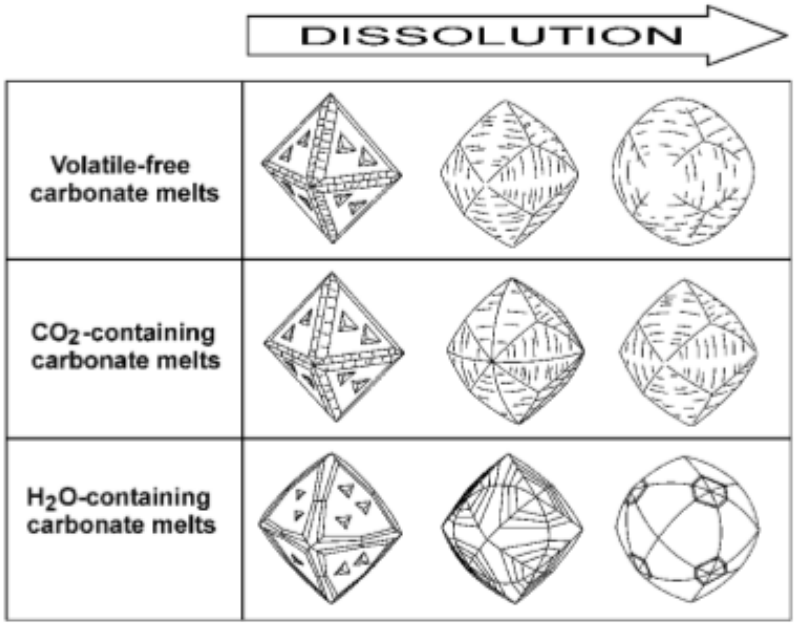

Figure 2.1.3. Morphological evolution schemes for octahedral diamonds in dry (volatile-free), CO_2-bearing, and H_2O-bearing carbonate melts. Khokhryakov and Palyanov (2010).

2.1.4 Factors affecting orientation of trigonal etch pits

Negatively oriented trigons are the most common type of etch pits on diamond surface, whereas positive trigons are very rare (Robinson, 1979). The crystal lattice of the [111] face of an octahedral diamond consists of alternating rows of carbon atoms bound to their three neighbours as well as the atoms from the [111] layer below and of carbon atoms only bound to their three neighbours and having one dangling bond (Figure 2.1.4) (Angus and Dyble, 1975). Three- and four-bonded atoms are harder to remove than two- or one-bonded atoms that surround the holes and defects, which results in triangular etch pits, or trigons, that can be formed by removing only two-bonded atoms (Angus and Dyble, 1975). Figure 2.1.4 shows that according to Angus and Dyble's proposed mechanism, negative trigons are easier to form than positive trigons because negative trigons only require the removal of doubly-bonded atoms, whereas positive trigons require the removal of three-bonded atoms (Angus and Dyble, 1975).

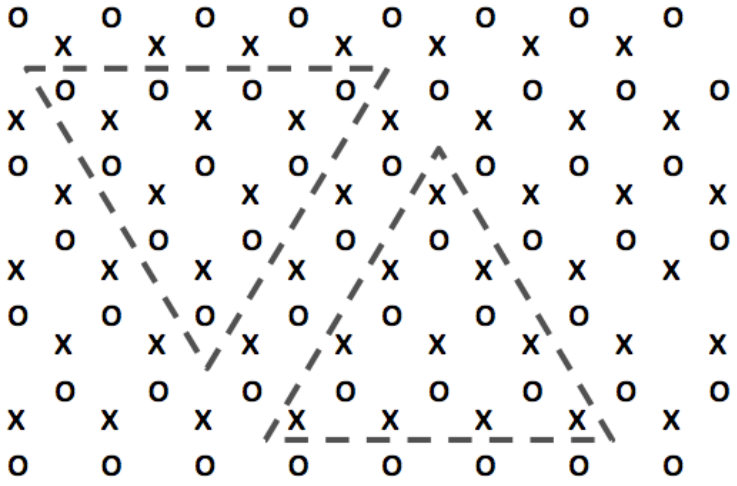

Figure 2.1.4. Schematic of carbon atoms on the diamond surface. Carbons bound to their three neighbours as well as the layer below are represented by Xs; carbons bound to their three neighbours only are represented by Os. Dashed lines show negative and positive trigons. The edges of negative trigons are defined by the removal of atoms not bound to the layer below, whereas positive trigons require the removal of atoms bound to the layer below. After Angus and Dyble (1975).

Studies have investigated the dependence of trigon orientation on oxidation conditions, and shown that orientation depends on temperature and oxygen fugacity (Yamaoka et al, 1980). Experiments were carried out at 15 kbar and 800-1400ºC with varying oxygen fugacity (Yamaoka et al, 1980). The results showed that negative trigon development favoured high temperature, and that as oxygen fugacity increased, the temperature required to produce negative trigons increased as well (Yamaoka et al, 1980). Yamaoka et al. (1980) proposed that at high oxygen fugacities, oxygen atoms form "bridges" between carbon atoms on the diamond surface that stabilize the walls of negative trigons, allowing dissolution to occur on walls of positive trigons instead.

The mechanism of trigon orientation is still not well understood, in part due to the lack of robust data on trigons. Gathering more detailed and precise measurements of trigons using atomic force microscopy (AFM) may shed more light on the mechanisms controlling trigon orientation.

2.2 Atomic force microscopy as a new method to study diamond resorption

The atomic force microscope, a type of scanning probe microscope, was invented in the 1980s and are used in a multitude of settings including surface science and 3D imaging. In Earth Sciences, they have previously been used to investigate mineral growth and dissolution (Dove and Blatt, 1995). Atomic force microscopy (AFM) can be used to map resorption features on the surface of diamonds and provide the means to precisely measure their size, shape, and depth, as well as other properties such as the slope of etch pit walls. These measurements facilitate the interpretation the geometry of resorption features and test models of their development mechanisms (Zhang et al, 2015).

Fedortchouk et al. (2011) used AFM to examine and measure dissolution features on [111] faces of diamonds, allowing a more quantitative description of features that previously had been described more qualitatively. Diamonds exposed to H_2O-rich fluid at 1150ºC–1350ºC generally formed large flat-bottomed trigons whose side lengths increased with increased temperature (Fedortchouk et al, 2011). Wall slope increased with increased trigon depth, the most common measurements being 7º, 11º, 16º, and 22º which correspond to the [433], [322], [221], and [321] diamond lattice directions respectively (Fedortchouk et al, 2011). In CO_2-rich fluid at 1250ºC diamonds developed numerous trigonal and hexagonal etch pits, including small point-bottomed trigons with steeper wall slopes (6ºC–36º) than trigons produced in H_2O-rich fluid (Fedortchouk et al, 2011). Some trigons had profiles intermediate between point-bottomed and flat-bottomed, which were described as round-bottomed and had longer side lengths than point-bottomed trigons (Fedortchouk et al, 2011). AFM analysis of a diamond that was resorbed in natural kimberlitic magma showed features similar to those produced in H_2O-rich fluids (Fedortchouk et al, 2011).

Using AFM, Fedortchouk (2015) found that the relationship between the depth and diameter of trigonal pits depends on the composition of diamond-destructive fluid, and can be used to constrain the conditions in natural diamond environments.

Zhang (2015) used profiles obtained with AFM to refine types of trigons based on their wall shape. Flat-bottomed trigons were divided into three categories: trapezoid-shaped trigons with constant wall slope, trumpet-shaped trigons with upper wall slopes lesser than their lower wall slopes, and rounded trigons with upper wall slopes greater than their lower wall slopes (Zhang, 2015). Point-bottomed trigons were divided into

two categories: trumpet-shaped trigons with upper wall slopes greater than their lower wall slopes, and V-shaped trigons with constant wall slope (Zhang et al, 2015). For the purposes of this study, a similar classification method was used to describe trigons. Those with constant wall slopes were defined as V-shaped, those with an upper wall slope lesser than the lower wall slope were defined as Y-shaped, and those with an upper wall slope greater than the lower wall slope were defined as U-shaped, as described in Li et al. (2015).

2.3 Background geology

2.3.1 Kimberlite geology and facies

The morphology of a kimberlite is usually a vertical carrot-shaped pipe along with tabular dikes called fissure kimberlites (Mitchell, 1986). There are three kimberlitic facies, based on texture and emplacement mechanism: crater, diatreme, and hypabyssal. The idealized model of kimberlite based on South African occurrences is shown on Figure 2.3.1.

Crater facies kimberlite occupies the crater lake formed at the top of the kimberlite pipe by its explosive eruption (Mitchell, 1986). It commonly consists of pyroclastic tuff and epiclastics that have been fluvially reworked. Rarely, crater facies also contains lava, the only example being in Igwisi Hills in Tanzania (Mitchell, 1986). Kimberlites usually produce pyroclastic deposits rather than lavas (Mitchell, 1986). Diatreme facies kimberlite forms the 1 to 2 km long pipe underlying the crater facies. The diatreme zone has roughly vertical walls and a elliptical to near-circular cross-sectional area that decreases with depth until it terminates at the root zone (Mitchell,

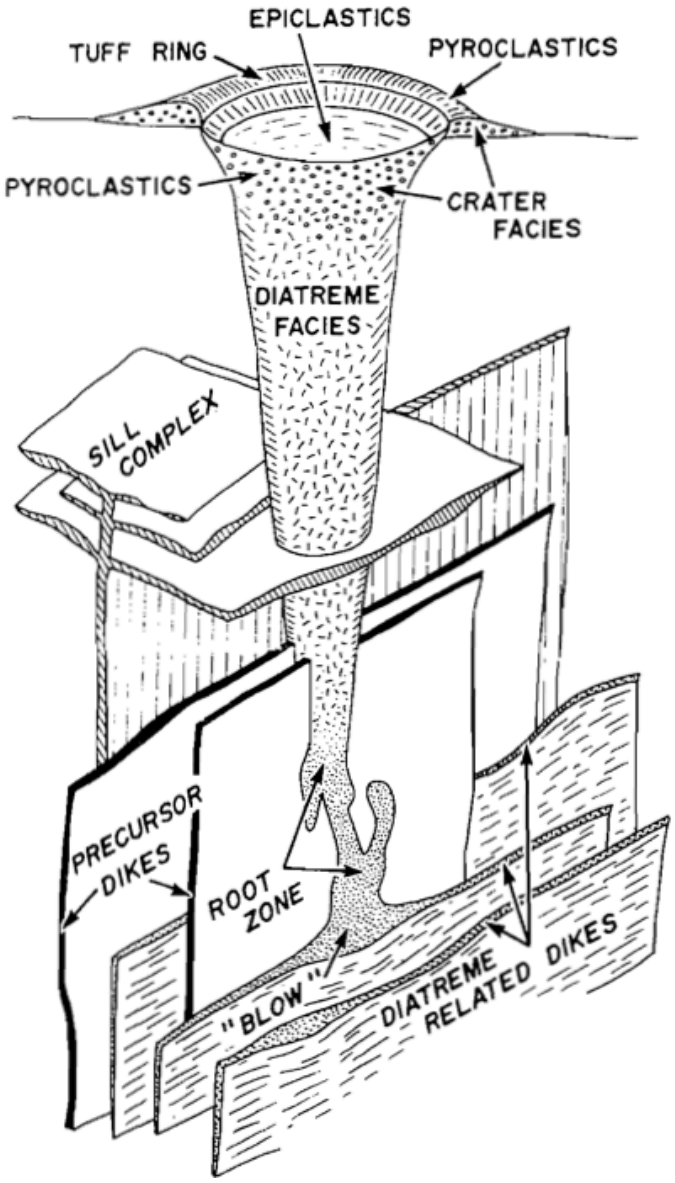

Figure 2.3.1. Idealized kimberlite pipe based on kimberlites from Southern Africa. Mitchell (1986).

1986). They are commonly tuffisitic kimberlite breccias that contain clasts of country rock inclusions, hypabyssal kimberlite autoliths, and olivine, garnet, and ilmenite grains (Mitchell, 1986). The groundmass is usually made up of diopside and serpentine, but has often been altered to clay minerals and secondary calcite (Mitchell, 1986). Hypabyssal or coherent facies kimberlite makes up the root zone of the kimberlite pipe and usually occurs as dikes and sills (Mitchell, 1986). It forms from the crystallization of kimberlitic

magma rich in volatiles. It often contains a large enough proportion of country rock inclusions to be considered a kimberlite breccia (Mitchell, 1986).

Canadian kimberlites show a large morphological diversity and do not always resemble kimberlites from Southern Africa. Field and Scott-Smith (1999) divided them into three types based on morphology: (1) large and shallow pipes filled with pyroclastic kimberlite, (2) small pipes with steep sides filled mainly with resedimented volcaniclastic kimberlite, and (3) small pipes with steep sides filled mainly with tuffisitic kimberlite breccia and hypabyssal kimberlite (Field and Scott-Smith, 1999). Scott-Smith (2008) suggests that the morphological differences are caused by different country rocks into which kimberlites are emplaced. Type 1 kimberlites occur where country rock is sedimentary; type 2 kimberlites occur where country rocks are granitoids covered by sedimentary rocks; and type 3 kimberlites occur where the country rock is all granitoid (Scott-Smith, 2008). Scott-Smith (2008) suggests that differences in country rocks affect the emplacement of kimberlites, resulting in different pipe morphologies.

Skinner and Marsh (2004) noted that there are some instances where different kimberlite morphologies occur in the same geologic setting and suggested that the differences could be due to different volatile compositions affecting emplacement style (Skinner and Marsh, 2004). They suggested that type 1 and 3 kimberlites result when kimberlites have a high H_2O content, causing magma to crystallize at depth and reaches the surface due to explosive eruption (Skinner and Marsh, 2004). In contrast, type 2 kimberlites result from magma reaching the earth's surface, which could be caused by high CO_2 content (Skinner and Marsh, 2004).

Kimberlites are a source of diamond because they occur on areas of cratonized crust. As the kimberlitic magma ascends through the craton, it entrains xenoliths that contain diamonds (Mitchell, 1986). Often these xenoliths disintegrate during this process and their contents including diamonds are dispersed into the magma, although occasionally they stay intact and may contain large quantities of diamond (Mitchell, 1986). Approximately 10% of kimberlites are diamondiferous, but only a small portion of them (<1%) contain enough diamonds to profitably mine them (Brooker, 2011; Mitchell, 1986). Despite this, kimberlites supply the majority of the world's natural diamonds.

2.3.3 Snap Lake kimberlite

The Snap Lake kimberlitic intrusion is located in the Northwest Territories of Canada, approximately 220 km north of Yellowknife (Gernon et al, 2012). The kimberlite is 535–523 Ma old (Gernon et al, 2012) and is composed of a series of interconnected 0.5–15 m thick subparallel dikes (Gernon et al, 2012), as opposed to the more common pipe-like morphology of kimberlites. The country rocks are of the Defeat Pluton suite containing granodiorites, tonalites, and granites, as well as metavolcanics of the Yellowknife Supergroup such as amphibolites, metaturbidites, and migmatites (Gernon et al, 2012). The regional stress regime most likely influenced the location and orientation of the kimberlite sheets, as they are parallel to the foliation of the metavolanics, primary joints in the granitoids, and tension stress fractures from reactivation of older faults (Gernon et al, 2012).

The Snap Lake kimberlite consists of one main hypabyssal kimberlite and two minor breccias. The hypabyssal kimberlite is xenolith-poor, with coarse-grained olivine macrocrysts and mantle-derived garnet xenocrysts in the groundmass (Kopylova, 2010). The groundmass is made up of olivine phenocrysts, phlogopite, former monticellite, spinel, rutile, ilmenite, carbonate, serpentine, and apatite (Kopylova, 2010). Olivine and monticellite have been replaced by serpentine and carbonate (Koplova, 2010). The breccias are highly altered, with amphibolite and granitic xenoliths and a matrix of serpentine, carbonate, and spinel (Kopylova, 2010).

Two emplacement models for the Snap Lake kimberlite exist. The first, called the monogenetic emplacement model, assumes that a single magma produced a main type of hypabysaal kimberlite, and changes in degrees and forms of alteration are explained by crustal contamination and secondary alteration (De Beers Internal Report). The second, called the polygenetic model, assumes that two distinct magmas that mixed and intruded simultaneously formed two lithofacies of hypabyssal kimberlite (De Beers Internal Report).

Li et al. (2015) used resorption features on Snap Lake diamonds to explore the reason for the presence of two different kimberlite types in Snap Lake. A unique feature of Snap Lake diamonds is widespread development of positive trigons, (Li et al, 2015). While the morphology of the common resorption feature, negative trigons, shows no association with the general diamond morhology, the morphology of the positive trigons was associated with general morphology of the diamonds. Diamonds with ditrigonal [111] faces and few U-shaped negative trigons had V- and U-shaped positive trigons that were shallow with longer side lengths (Li et al, 2015). Diamonds with ditrigonal [111]

faces and no negative trigons had deeper V-shaped positive trigons (Li et al, 2015). Diamonds with trigonal [111] faces and numerous Y-shaped negative trigons had V- and U-shaped positive trigons (Li et al, 2015). Diamonds with ditrigonal [111] faces and Y-shaped trigons and hexagons had deep Y-shaped positive trigons (Li et al, 2015). Li et al. (2015) suggested that Snap Lake diamonds showed three distinct evolution trends of positive trigons: V-shaped flat-bottomed to V-shaped point-bottomed, Y-shaped flat-bottomed to Y-shaped point-bottomed to Y-shaped flat bottomed, and flat-bottomed to U-shaped point-bottomed (Li et al, 2015). These evolution trends are thought to represent two distinct resorption conditions in the Snap Lake kimberlite, the first being at depth and the second being near the end of kimberlite emplacement (Li et al, 2015).

CHAPTER 3: SAMPLES AND METHODS

3.1 Diamond samples

The diamonds used in this study are from a diamond mine in Yakutia, Russia. They are octahedral white diamonds with minimal resorption features. See Table 3.1 for a description of the samples before experiments. AFM scans were done on one face of each diamond prior to the experiments to record any pre-existing features. See the

Table 3.1. Description of samples before experiments.

Sample	EK-1	EK-2	EK-3
Shape	Octahedral	Octahedral	Octahedral
Colour	White	White	White
Weight (mg)	1.08	0.82	0.45
Growth features present	Triangular plates	Triangular plates	Triangular plates
Resorption features present	Shield-shaped laminae	1 large, deep negative trigon Shield-shaped laminae	Few small, shallow negative trigons

appendix for microphotographs of the chosen faces for each sample.

3.2 Experimental methods

The diamond crystals were first cleaned by placing them into a beaker filled with ethanol inside a Branson 1510 Ultrasonic cleaner for 30 minutes to remove dust or dirt from the sample surfaces. They were then weighed and each face of each sample was photographed under a petrographic microscope in reflected light.

The starting mixtures used powders of reagent grade Na_2CO_3, NaCl, and NaF. The diamonds were placed on the bottom of a 25 mL Al_2O_3 crucible with the face of interest facing up to ensure that it was exposed to the melt. The crucible was then filled with 5 g of the starting mixtures by adding Na_2CO_3 first and NaCl or NaF second in the required proportions (Table 3.2). Pure Na_2CO_3 was used in experiment with diamond EK-1, mixture of Na_2CO_3 and NaCl with diamond EK-2, and mixture of Na_2CO_3 and NaF with diamond EK-3.

The crucibles were placed in a Ney Vulcan 3-550 furnace at 950ºC for 1 hour and each composition was studied in three consequent runs. The temperature was chosen to ensure that it was above the melting temperature for the three systems based on the melting temperature of Na_2CO_3 and the phase diagrams for Na_2CO_3-NaCl and Na_2CO_3-NaF systems (Fig. 3.2). After the crucibles were cooled down, the samples extracted from the melt were inspected for the presence of any surface graphitization, then cleaned by boiling in a mixture of H_2SO_4 and HNO_3 acids in a 5:3 volume ratio to remove any graphite followed by cleaning in ethanol. Photographs were taken of every face on each sample under an optical microscope in reflected light, and then each sample was mounted

Table 3.2. Melt compositions and masses of individual components.

Sample	Melt composition	Component	mol %	Mass (g)
EK-1	Na_2CO_3	Na_2CO_3	100	5.0000
EK-2	Na_2CO_3-NaCl	Na_2CO_3	70	4.0436
		NaCl	30	0.9564
EK-3	Na_2CO_3-NaF	Na_2CO_3	70	4.2742
		NaF	30	0.7258

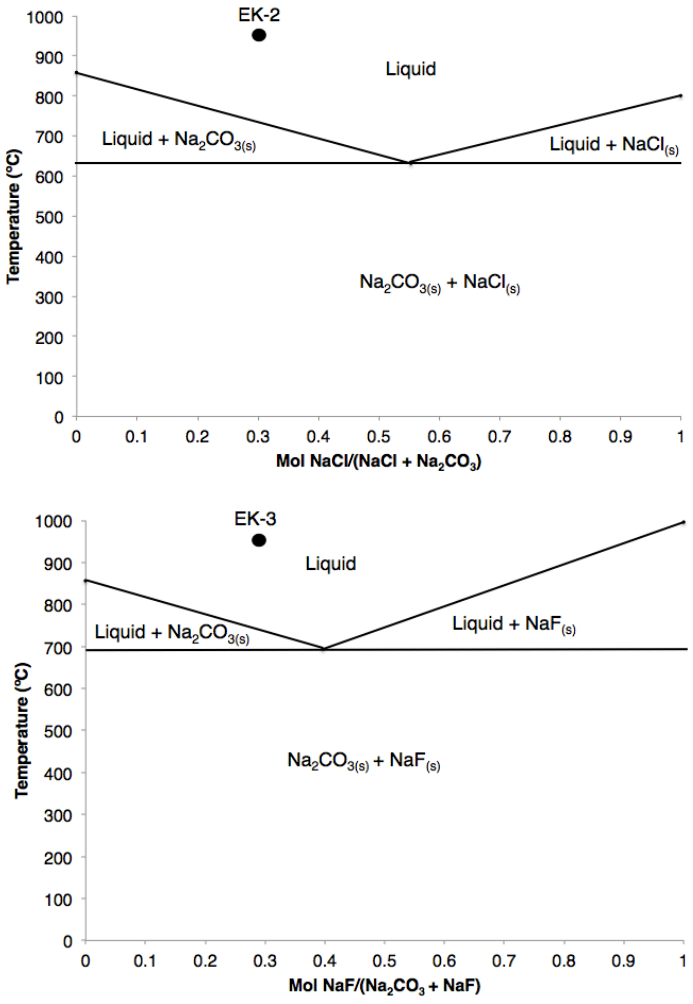

Figure 3.2. Phase diagrams for $NaCO_3$-NaCl and $NaCO_3$-NaF melts. Dots represent melt composition and temperature conditions for experiments on EK-2 and EK-3.

on a metal plate for the AFM analysis.

After run 1 and run 2 at least ten newly formed trigons were mapped using the AFM on each diamond crystal. Samples with several populations of trigons with different sizes and/or shapes had ten trigons of each population mapped. An effort was made to scan the same features and the same areas of [111] diamond faces to examine the evolution of the resorption features in consequent experiments. After run 3, diamonds were cleaned, weighed, and photographed, but not scanned with AFM.

3.3 Atomic force microscopy

3.3.1 Overview of AFM

Atomic force microscopy (AFM) is a type of scanning probe microscopy that can map the surface of materials at extremely high resolutions, even down to the atomic level (Howland and Benatar, 2000). The microscope consists of a microns-long tip (Fig. 3.3.1.1) that can have a diameter of less than 100 angstroms attached to a cantilever that is only 100 to 200 μm long (Howland and Benatar, 2000). When brought near the surface of a material, the cantilever is deflected by forces between the tip and the sample surface (Howland and Benatar, 2000). A detector measures the amount of deflection and this information allows a computer to produce a map of the sample surface (Howland and Benatar, 2000). Figure 3.3.1.2 shows a simplified schematic of an AFM. The force that acts upon the cantilever is most commonly the Van der Waals, or interatomic, force (Howland and Benatar, 2000), that occurs between the tip and the sample due to the

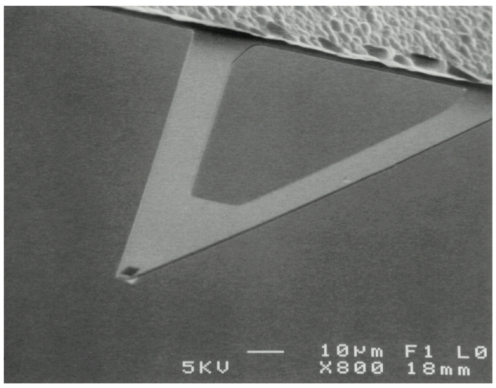

Figure 3.3.1. A silicon nitride cantilever used for contact mode AFM (Veeco, 2010)

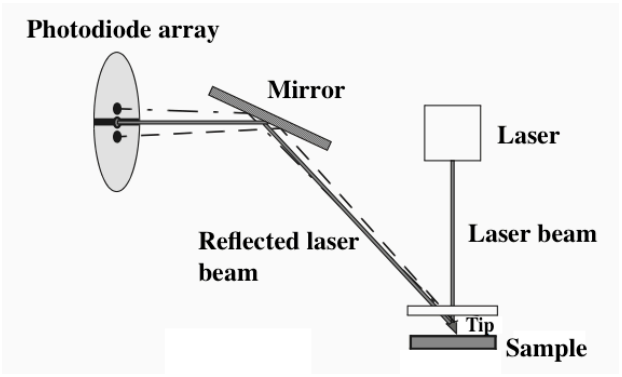

Figure 3.3.2. A simplified schematic of an AFM. A laser beam is reflected off the cantilever and is directed to a photodiode array to measure the amount cantilever deflection (adapted from Veeco, 2010).

attraction and repulsion between their respective molecules. AFM produces a high-resolution map of the microscopic-scale topography of the sample surface.

AFM scans may be carried out in two modes: contact mode and tapping mode. In contact mode, the tip is in continuous direct contact with the sample surface. Contact mode cantilevers are usually made of silicon nitride, as they are very flexible (Veeco, 2010). In tapping mode, the cantilever oscillates so that the tip contacts the sample surface in a series of tapping motions (Veeco, 2010). Tapping mode cantilevers are usually made of an etched crystal silicon tip, which is stiffer than a silicon nitride tip (Veeco, 2010).

3.3.2 Analytical parameters

Trigons and other features on the face of interest of each diamond were mapped using a Bruker MultiForce 8 AFM at Dalhousie University on contact mode. The tip used was a silicon nitride tip with a spring constant of 0.2-0.8 N/m, a resonant frequency of 45-95 kHz, a nominal tip radius of curvature of 2 nm, and a length of 115 μm. Scan

map areas were between 10 μm^2 and 50 μm^2, depending on the size of the trigon or feature being mapped. To reduce piezoelectricity arising from the stresses applied to the microprobe tip during scanning, scanning rates for larger map areas or areas containing deep features must be lower (Veeco, 2010). Scan rates were between 0.3 Hz and 0.6 Hz, depending on the size of the scan area and depth of features.

3.3.3 Data processing and uncertainties

Scan maps were processed using NanoScope software 8.10. Each map was first fit to a horizontal plane and three cross section profiles were drawn through each trigon. Diameter, depth, wall slope, and wall shape were measured for each trigon.

Uncertainties in the data arise from three sources: uncertainty inherent to the AFM, selection of measurement points, and angle of the diamond face. The accuracy of the AFM in the x, y, and z direction is +/- 1.4% (Zhang et al, 2015). Selection of measurement points on cross section profiles is subjective and introduces an uncertainty of +/- 1%. After the scan map is fitted to a horizontal plane, it may still be at a small angle (<1º) relative to horizontal, which causes an uncertainty of +/- 0.2º in angle measurements. The total uncertainty for distance measurements was +/- 2.4% and for angle measurements +/- 0.2º.

CHAPTER 4: RESULTS

4.1 Evolution of diamond morphology

All diamonds experienced resorption at the run conditions, evidenced by their weight loss. All diamonds developed positive trigons, but the distribution, size, and

Table 4.1. Diamond weight loss after experimental runs and dissolution rates. Dissolution rates in mg/(hr*mm^2) take into account the different starting weights of each diamond.

Diamond	Melt Composition	Weight, start (mg)	Weight, run 1 (mg)	Weight, run 2 (mg)	Weight, run 3 (mg)	Dissolution rate (mg/hr)	Dissolution rate (mg/(hr*mm^2))
EK-1	Na_2CO_3	1.08	1.04	1.02	0.99	0.030	0.011
EK-2	Na_2CO_3-NaCl	0.82	0.79	0.78	0.72	0.033	0.014
EK-3	Na_2CO_3-NaF	0.45	0.41	0.39	0.35	0.033	0.021

morphology of trigons differed between melt compositions. Table 4.1 records weight loss and dissolution rate for each diamond.

4.1.1 Sample EK-1 in Na_2CO_3 melt

Run 1

After exposure to a Na_2CO_3 melt for 1 hour, EK-1 lost 3.7% of its mass indicating that resorption occurred. Side length decreased by 1.2% and the edges and corners of the [111] face became slightly rounded, resulting in a 3.7% loss of area. The [111] face became covered in numerous positive flat-bottomed trigons of various depths that were distributed fairly evenly across the surface with the exception of being sparse in one corner.

Run 2

After exposure to a Na_2CO_3 melt for 2 hours, EK-1 lost 5.6% of its mass, 3.2% of its side length, and 13.8% of its [111] area. The number and size of the positive flat-bottomed trigons on [111] face increased notably. Figure 4.1.1 shows microphotographs and AFM scans of the [111] face, showing how the morphology evolved over the course of the two runs.

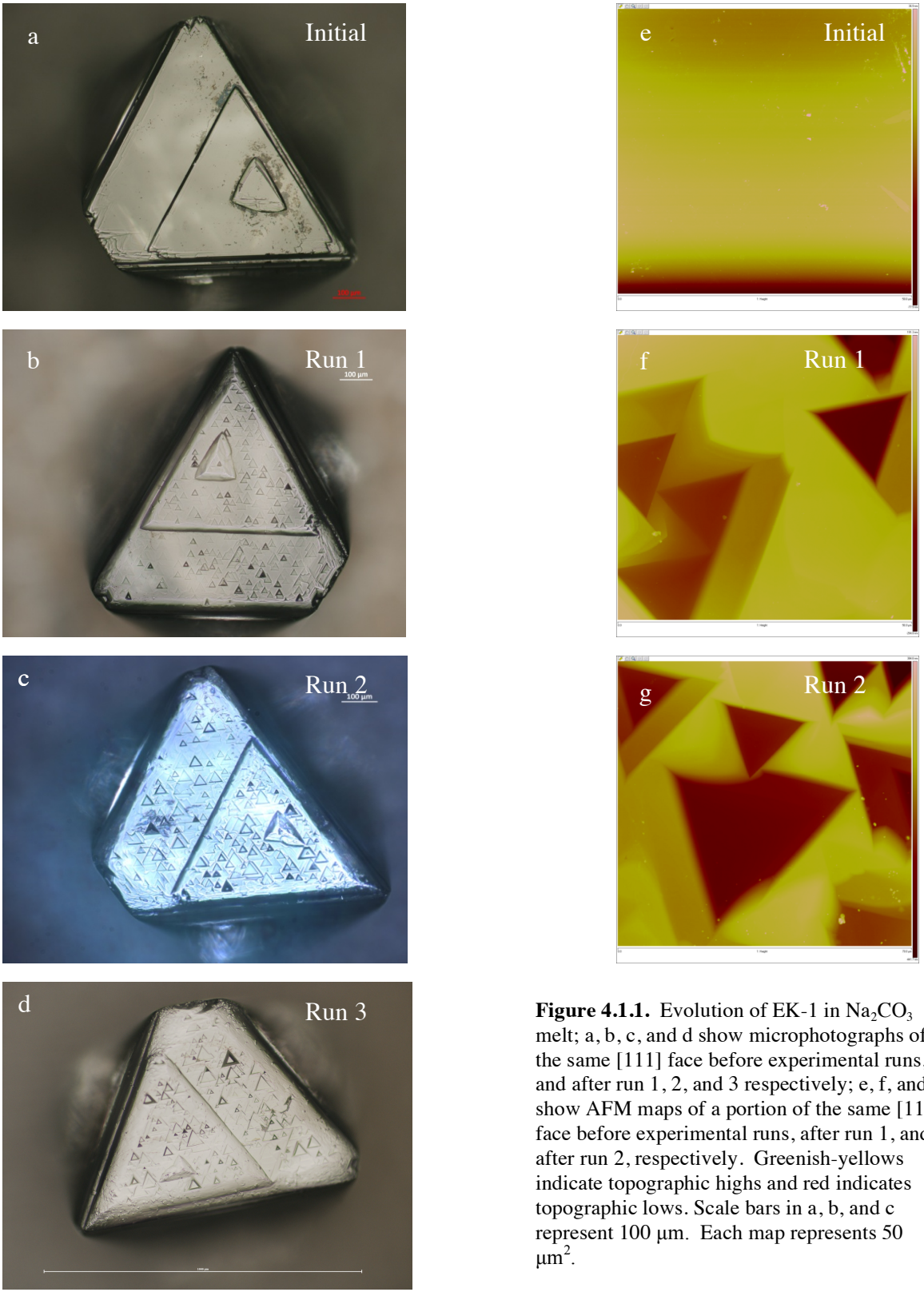

Figure 4.1.1. Evolution of EK-1 in Na_2CO_3 melt; a, b, c, and d show microphotographs of the same [111] face before experimental runs, and after run 1, 2, and 3 respectively; e, f, and g show AFM maps of a portion of the same [111] face before experimental runs, after run 1, and after run 2, respectively. Greenish-yellows indicate topographic highs and red indicates topographic lows. Scale bars in a, b, and c represent 100 µm. Each map represents 50 μm^2.

4.1.2 Sample EK-2 in Na_2CO_3-NaCl melt

Run 1

After exposure to a Na_2CO_3-NaCl melt for 1 hour, EK-2 lost 3.7% of its mass. Side length, measured with ImageJ software, decreased by 1.4% and the area of the [111] face decreased by 1.1%, while the sides and corners showed no traces of rounding. The large negative trigon that was initially present on this diamond developed truncated corners and increased its side length from 188 to 193 μm. Large circular features with a ~450 μm diameter developed in the center of two opposite [111] faces covering most of their surfaces. The side studied on AFM (Fig. 4.1.1) has large flat-bottomed and point-bottomed positive trigons developed inside this circular feature. Smaller flat- and point-bottomed positive trigons developed at the corners of the [111] face outside the circular feature. Lines of overlapping trigons developed at numerous locations on the face. On the opposite side, there was no relationship between the circular feature and trigon size.

Run 2

After exposure to a Na_2CO_3-NaCl melt for 2 hours, EK-2 lost 5% of its mass in total. Side length decreased by 0.2% and the area of the [111] face decreased by 2.4%. The sides and corners of the diamond showed no rounding. The side length of the large negative trigon increased by 3.8% and the truncated corners grew more pronounced. The diameter of the large circular feature did not change. The [111] face was covered in predominantly flat-bottomed positive trigons, with some minor point-bottomed positive trigons. As seen after run 1, the area of the face inside the circular feature developed larger trigons than the area of the face outside the circular feature, and lines of overlapping trigons persisted (Figure 4.1.2).

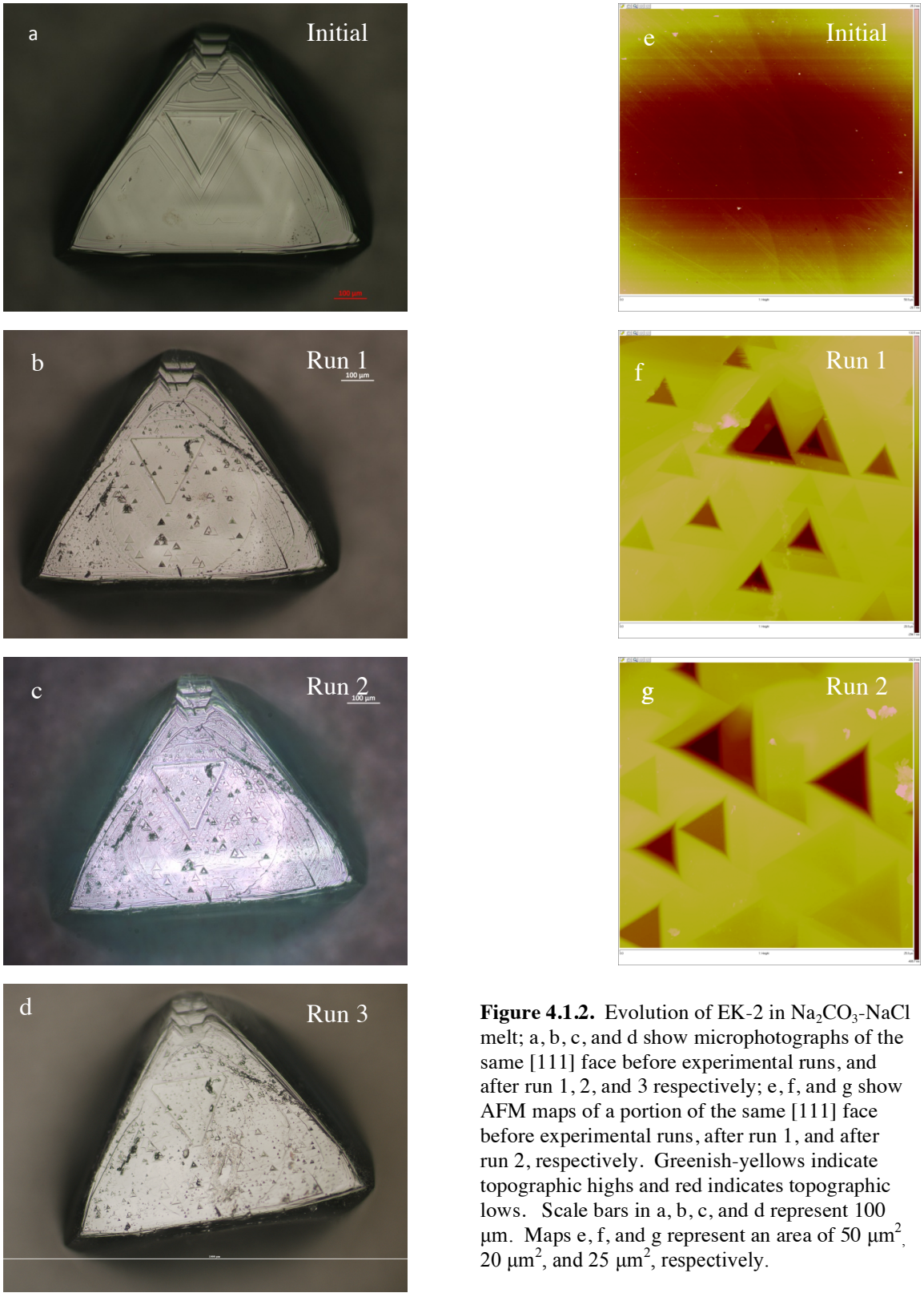

Figure 4.1.2. Evolution of EK-2 in Na_2CO_3-NaCl melt; a, b, c, and d show microphotographs of the same [111] face before experimental runs, and after run 1, 2, and 3 respectively; e, f, and g show AFM maps of a portion of the same [111] face before experimental runs, after run 1, and after run 2, respectively. Greenish-yellows indicate topographic highs and red indicates topographic lows. Scale bars in a, b, c, and d represent 100 µm. Maps e, f, and g represent an area of 50 μm^2, 20 μm^2, and 25 μm^2, respectively.

4.1.3 Sample EK-3 in Na_2CO_3-NaF melt

Run 1

After an exposure to a Na_2CO_3-NaF melt for 1 hour, EK-3 lost 8.9% of its mass. Side length decreased by 2.2% and the area of the [111] face decreased by 1.3% with slight rounding of the edges and corners. The [111] face was covered in numerous flat- and point-bottomed positive trigons. The few shallow negative trigons that were present initially could not be located.

Run 2

After exposure to a Na_2CO_3-NaF melt for 2 hours, EK-3 lost 13.7% of its mass in total. Side length decreased by 3.1% and the area of the [111] face decreased by 3.6%. The edges and corners of the diamond remained slightly rounded. The [111] face was covered with flat- and point-bottomed positive trigons. The size of these trigons did not change significantly, but the abundance slightly increased (Figure 4.1.3).

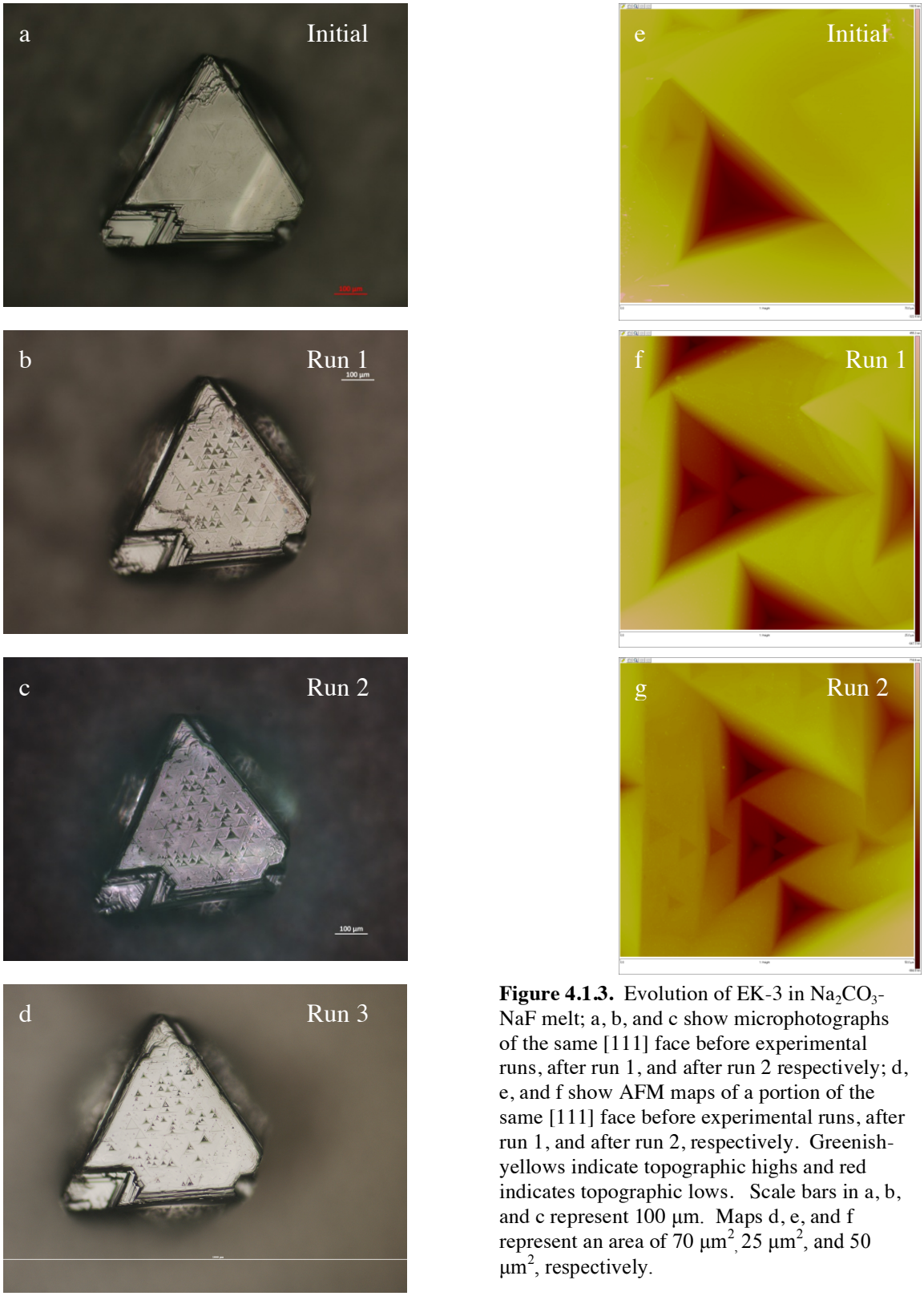

Figure 4.1.3. Evolution of EK-3 in Na_2CO_3-NaF melt; a, b, and c show microphotographs of the same [111] face before experimental runs, after run 1, and after run 2 respectively; d, e, and f show AFM maps of a portion of the same [111] face before experimental runs, after run 1, and after run 2, respectively. Greenish-yellows indicate topographic highs and red indicates topographic lows. Scale bars in a, b, and c represent 100 µm. Maps d, e, and f represent an area of 70 μm^2, 25 μm^2, and 50 μm^2, respectively.

4.2 Kinetics of diamond dissolution

Table 4.2 summarizes the % weight loss, % [111] area decrease, and vertical dissolution depth for each melt. Diamonds lost between 2 and 4 mg per run. [111] area decreased between run 1 and run 2 for every diamond. EK-1 in Na_2CO_3 had the lowest total weight loss after three runs, but the highest total [111]area decrease and the greatest vertical dissolution between runs 1 and 2. EK-2 in Na_2CO_3-NaCl had intermediate total weight loss and total [111] area decrease, but the smallest amount of vertical dissolution. EK-3 in Na_2CO_3-NaF had the highest total weight loss, the lowest total [111] area loss, and an intermediate amount of vertical dissolution between runs 1 and 2.

Figure 4.2a shows the relationship between % weight loss and run duration for each diamond and melt composition. Despite the differences in % weight loss, the dissolution rate for all diamonds was between 0.31–0.32 mm/hr, indicating that the difference in % weight loss is due to the differences in starting weight of the diamonds. Figure 4.2b shows the relationship between % [111] area decrease and run duration for each diamond and composition. EK-1 in Na_2CO_3 had a much higher [111] area decrease than EK-2 in Na_2CO_3-NaCl and EK-3 in Na_2CO_3-NaF due to the higher degree of rounding that occurred during dissolution of EK-1 compared to EK-2 and EK-3.

Table 4.2. Summary of diamond weight loss, [111] area loss, and vertical dissolution between run 1 and run 2. % area loss refers to the area of one [111] face.

Diamond	% wt. loss, Run 1	% wt. loss, Run 2	% wt. loss, Run 3	% [111] area loss, Run 1	% [111] area loss, Run 2	% [111] area loss, Run 3	Vertical dissolution between Runs 1 and 2, nm
EK-1	3.7	5.6	8.3	3.7	13.8	19.8	439
EK-2	3.7	5.1	12.2	1.1	3.5	9.0	140
EK-3	8.9	14.6	22.2	1.3	4.8	7.5	296

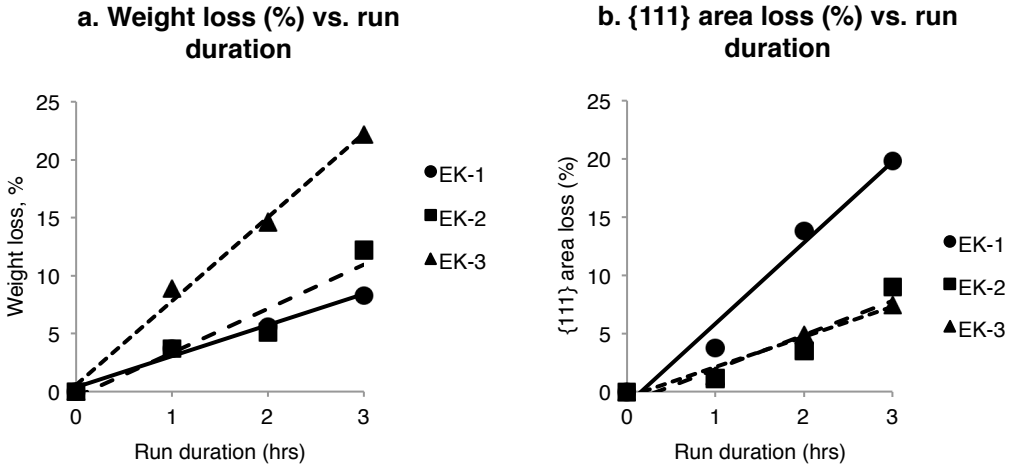

Figure 4.2. (a) Weight loss (%) vs. run duration. (b) [111] area loss (%) vs. run duration. EK-1, EK-2, and EK-3 are represented by circles with black lines, squares with dashed lines, and triangles with dotted lines respectively.

4.3 AFM study of trigonal etch pits

Table 4.3 summarizes the average diameter, depth, and wall shape of trigons from each diamond. Flat-bottomed trigons showed a range of sizes that could be divided into two groups based on their diameter. Most flat-bottomed trigons had Y-shaped walls. Point-bottomed trigons could be divided into two groups based on diameter after run 1, but after run 2 were confined to one size range. Most point-bottomed trigons had Y-shaped walls.

The trigons that developed on EK-1 after run 1 (Figure 4.3.1) were all of very similar diameter, ranging from 17.8 to 24.0 μm. Depths varied from 82 to 944 nm. They were all flat-bottomed and had pronounced Y-shaped walls. On EK-1, all trigons are flat-bottomed with Y-shaped walls, and the average diameter and depth increased from run 1 to run 2. There was a weak correlation between increased diameter and increased depth, and there were no distinct size groups.

Table 4.3. Trigon diameter, depth, and shape for each diamond after runs 1 and 2. Trigons on EK-2 were split into two groups based on size. Trigons on EK-3 were split into two groups based on bottom shape.

Diamond	Average trigon diameter, run 1, μm	Average trigon diameter, run 2, μm	Average trigon depth, run 1, nm	Average trigon depth, run 2, nm	Trigon shape, run 1	Trigon shape, run 2
EK-1	20.8	27.6	278	292	Y-shaped Flat-bottomed	Y-shaped Flat-bottomed
EK-2	Large 20.6 Small 3.5	Large 22.6 Small 6.3	Large 617 Small 160	Large 592 Small 205	Y-, U-, V-shaped Flat-, point-, round bottomed	Y-, U-, V-shaped Flat-, point-, round bottomed
EK-3	Flat 19.2 Point 19.8	Flat 26.4 Point 25.1	Flat 419 Point 908	Flat 412 Point 1157	Y-shaped Flat-, point-bottomed	Y-shaped Flat-, point-bottomed

The trigons that developed on EK-2 after run 1 (Figure 4.3.2) showed a wide range of diameters, depths, bottom shapes, and wall shapes, however some trends appear when they are considered in terms of their relationship to the large circular feature in the center of the [111] face. The trigons inside the circular feature, called group 1 trigons, ranged from 16.4 to 27.4 μm in diameter and 244 to 1337 nm in depth. They were flat- and round-bottomed and had U-, Y-, and V-shaped walls. The average upper wall slope to lower wall slope ratio was 0.92. The trigons outside the circular feature, called group 2 trigons, ranged from 2.5 to 5.6 μm in diameter and 61 to 279 nm in depth. They were flat-bottomed with Y-shaped walls. Trigons on EK-2 can be split into two groups based on whether they were inside or outside the circular feature. Trigons inside the circular feature were flat- or round-bottomed and had U-, Y-, and V-shaped walls. Although their average diameter increased from run 1 to run 2, their average depth decreased, being the only group of trigons to do so. Group 1 trigons, being larger in diameter, were deeper

than group 2 trigons that had smaller diameters, however there was no strong correlation between depth and diameter within the individual groups. Trigons outside the circular feature were flat-bottomed and had Y-shaped walls. Although their morphology was similar to trigons formed on EK-1, these trigons were much smaller in diameter. Their average diameter and depth increased from 3.5 μm and 160 nm to 6.3 μm and 205 nm between run 1 and run 2.

The trigons that developed on EK-3 (Figure 4.3.3) were grouped based on their bottom shape. Run 1 developed shallower flat-bottomed trigons ranging from 11.5 to 29.4 μm in diameter and 195 to 684 nm to depth and all Y-shaped; and the deeper point-bottomed trigons ranged from 17.8 to 21.8 μm in diameter and 809 to 1043 nm in depth with Y-shaped walls. The point-bottomed trigons for the same diameter are much deeper than the flat-bottomed trigons. Flat-bottomed trigons after run 2 ranged from 16.9 to 42.5 μm in diameter and 236 to 1009 nm in depth, and all had Y-shaped walls. Point-bottomed trigons ranged from 22.8 to 28.5 μm in diameter and 1020 to 1274 nm in depth, with Y-shaped walls. The point-bottomed trigons continued to be smaller in diameter but still slightly deeper than flat-bottomed trigons. Trigons on EK-3 were point- and flat-bottomed and had Y-shaped walls. Their diameter and depth increased from 19.4 μm and 594 nm to 24.8 μm and 702 nm between run 1 to run 2.

Figure 4.3.4 shows the diameter-depth relationship for groups of trigons on each diamond. Overall, trigons with larger diameters had greater depths. There was no overall correlation between morphology and dimensions.

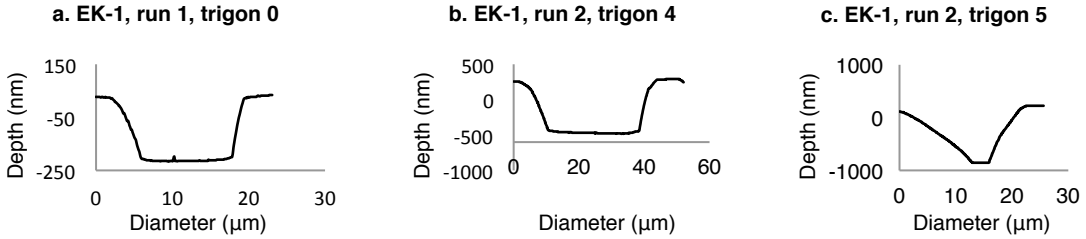

Figure 4.3.1. Trigons in EK-1 in Na_2CO_3 melt, scanned using an AFM. (a) shows a typical trigon after run 1. Trigons were flat bottomed with Y-shaped walls. (b) and (c) show typical trigons after run 2. Trigons are flat-bottomed with Y-shaped walls. Some trigons, as in (c), have narrower bottoms.

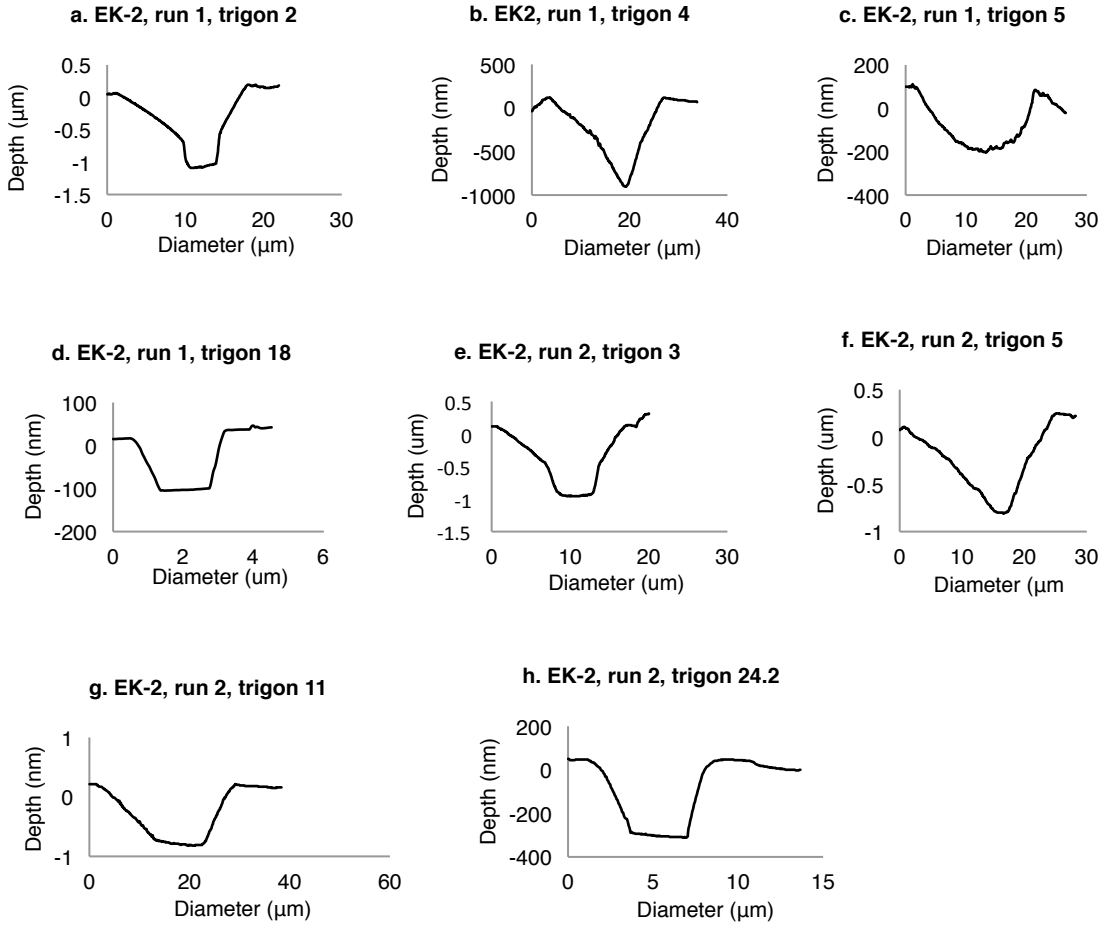

Figure 4.3.2. Trigons in EK-2 in Na_2CO_3-NaCl melt scanned using an AFM. a–d show trigons after run 1. (a) Y-shaped flat-bottomed. (b) Y-shaped point-bottomed. (c) U-shaped round bottomed. (d) V-shaped flat bottomed. e–h show trigons after run 2. (e) Y-shaped flat bottomed. (f) Y-shaped point-bottomed. (g) V-shaped flat bottomed. (h) V-shaped flat-bottomed. (d) and (h) have drastically smaller diameters. These trigons were located outside the circular feature in the centre of the diamond.

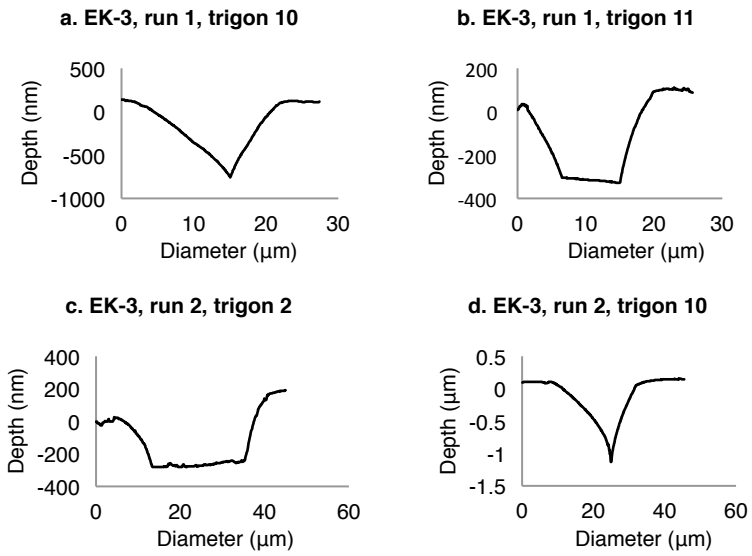

Figure 4.3.3. Trigons in EK-3 in Na_2CO_3-NaF melt scanned using an AFM. (a) and (b) show trigons from run 1. (a) V-shaped point-bottomed. (b) Y-shaped flat-bottomed. (c) and (d) show trigons from run 2. (c) Y-shaped flat-bottomed. (d) Y-shaped point-bottomed trigon.

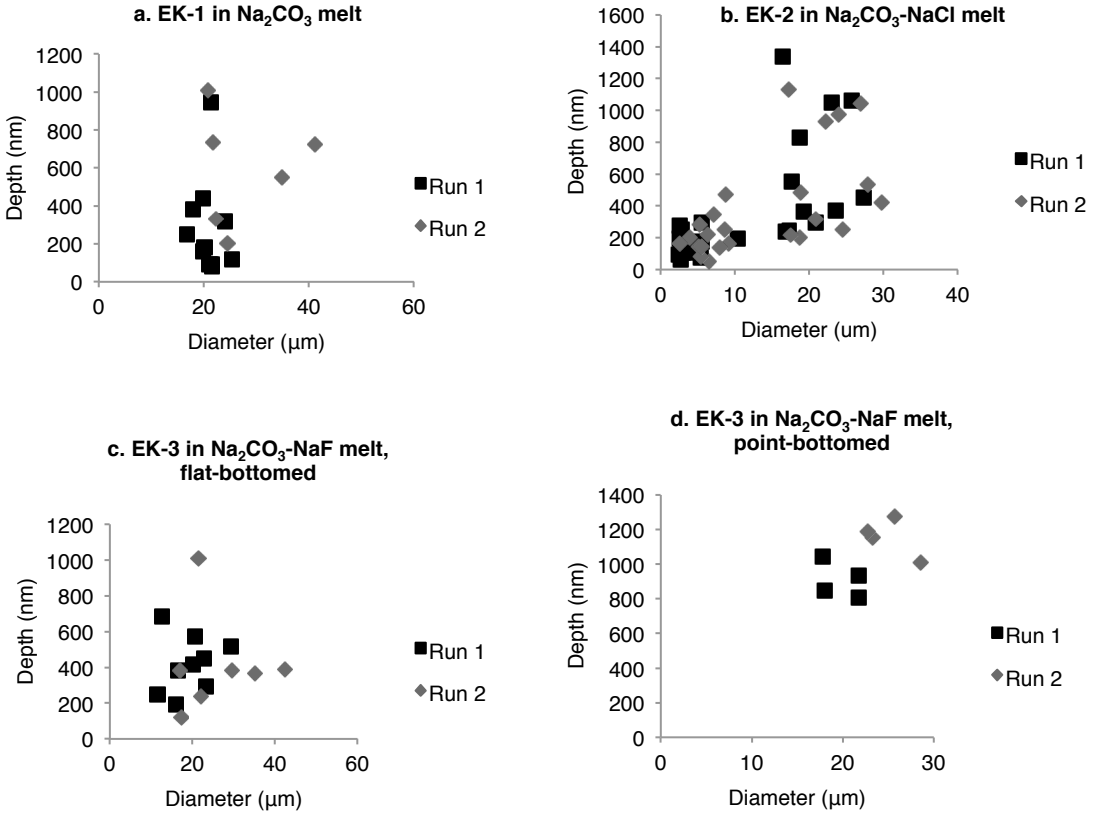

Figure 4.3.4. Diameter-depth relationships for trigons on each diamond after run 1 and run 2. Black squares represent trigons after run 1 and grey diamonds represent trigons after run 2. Trigons on EK-3 were split into two groups based on bottom shape.

4.4 Growth and evolution of trigonal etch pits during diamond dissolution

4.4.1 EK-1 in Na_2CO_3 melt

After run 2 an effort was made to scan the same trigons that were scanned after run 1, but significant resorption in [111] direction had removed most of the previously scanned trigons. Only the deepest trigon from run 1 could be identified. I estimated at least 439 nm of vertical resorption occurred on the [111] face, based on the maximum depth of a trigon from run 1, which disappeared after run 2. The range of trigon diameter increased to 21.6 to 39.3 μm. Depths varied from 199 to 1010 nm. They all remained flat-bottomed with Y-shaped walls. Figure 4.3.1 shows representative trigon profiles from run 1 and run 2.

Figure 4.4.1 shows the profile of the trigon that could be followed from run 1 to run 2. After both runs, the trigon is flat-bottomed with Y-shaped walls. The diameter increased from 21.3 μm to 29.9 μm, and the depth decreased from 944 nm to 505 nm, likely due to vertical resorption.

4.4.2 EK-2 in Na_2CO_3-NaCl melt

Almost every trigon scanned after run 1 was still present after run 2. The minimum amount of vertical resorption was 140 nm, determined by the minimum amount of vertical distance the surface must have moved so that the bottom of trigons scanned after run 2 were not above the bottom of trigons scanned after run 1. After run 2, group 1 trigons ranged from 17.2 to 29.8 μm in diameter and 198 to 1133 nm. They were flat- and round-bottomed and had U-. Y-, and V-shaped walls. Group 2 trigons ranged from 2.5 to 9.2 μm in diameter and 53 to 468 nm in depth. They all remained flat-bottomed

with Y-shaped walls. Figure 4.3.2 shows representative trigon profiles for groups 1 and 2 from run 1 and 2.

Following the same trigons between run 1 and run 2 showed that trigons maintained their morphology after both runs. Figure 4.4.2 shows overlain profiles after run 1 and run 2 for individual trigons. Trigon diameter increased by an average of 2 μm and depth decreased by 25.8 nm. In one case (Fig. 4.4.2), where the bottom of the trigon was narrow after run 1, the bottom became significantly wider with virtually no change in depth after run 2.

4.4.3 EK-3 in Na_2CO_3-NaF melt

After run 2, it was possible to identify 11 of 13 trigons scanned after run 1. The minimum amount of vertical resorption was 296 nm, based on the deepest trigon from run 1 that disappeared after run 2. . Figure 4.3.3 shows representative flat- and point-bottomed trigons from run 1 and 2. Figure 4.4.3 shows overlain profiles of trigons that could be followed between run 1 and run 2. In general, trigons maintained their morphology after both runs. The diameter of flat-bottomed trigons increased by an average of 7.2 μm and depth decreased by an average of 6.3 nm. The diameter of point-bottomed trigons increased by 5.3 μm and depth increased by 248 nm.

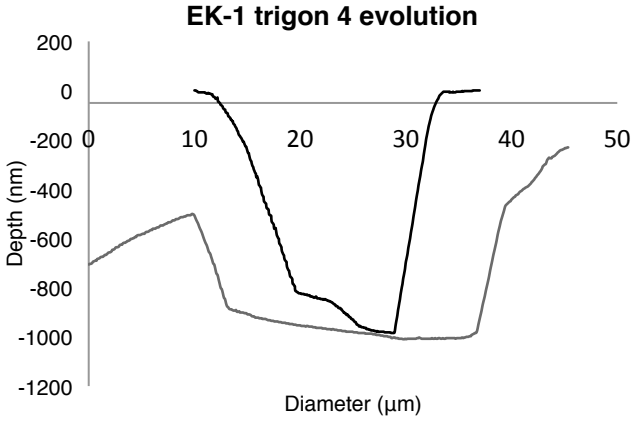

Figure 4.4.1. Trigon evolution on EK-1 in Na_2CO_3 melt. Black line represents trigon after run 1; grey line represents trigon after run 2. The trigon remained flat-bottomed, but its bottom widened after consequent runs.

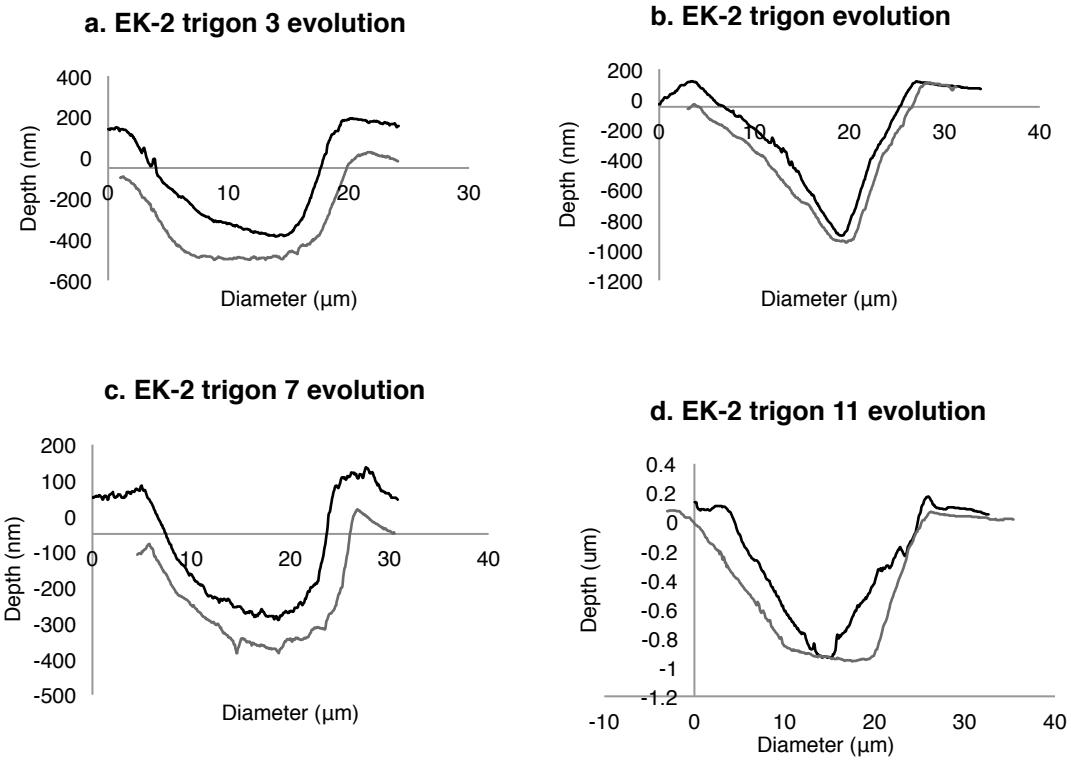

Figure 4.4.2. Trigon evolution on EK-2 in Na_2CO_3-NaCl melt. Black lines represent trigons after run 1; grey lines represent trigons after run 2. Trigons retained the same morphology after consequent runs. In the case of (d), the bottom remained flat, but also widened after run 2.

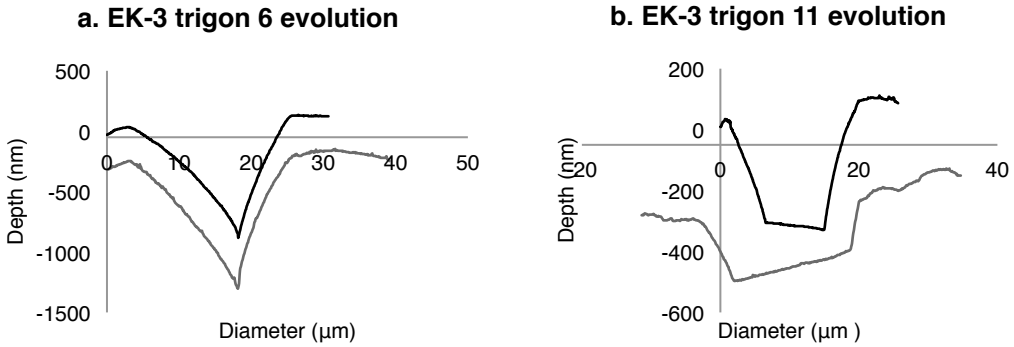

Figure 4.4.3. Trigon evolution on EK-3 in Na_2CO_3-NaF. Blck line represents trigons after run 1; grey lines represent trigons after run 2. Trigons maintained the same morphology between runs 1 and 2.

4.4.4 Summary

Diamond dissolution in Na_2CO_3 melt (EK-1) developed only one type of positive trigons: flat-bottomed trigons with Y-shaped walls. As runs progressed, diameter and depth of trigons increased, while morphology remained the same. The minimum amount of vertical resorption between run 1 and run 2 was determined to be 439 nm, the greatest of all three samples.

Diamond dissolution in Na_2CO_3-NaCl melt (EK-2) developed two groups of trigons based on their relationship to the large circular feature in the center of the [111] face. Group 1 trigons were larger than group 2 trigons and had flat-, round-, and point-bottoms. Group 2 trigons were confined to small, flat-bottomed trigons with Y-shaped walls. The depth of group 1 trigons decreased as run progressed, whereas the depth of group 2 trigons increased. The minimum amount of vertical resorption between run 1 and run 2 was 140 nm.

Diamond dissolution in Na_2CO_3-NaF melt (EK-3) developed flat- and point-bottomed trigons which remained as their respective morphologies as runs progressed. In general, flat-bottomed trigons had larger diameters and shallower depths than point-

bottomed trigons, which had small diameters but deeper depths. The minimum amount of vertical resorption between run 1 and run 2 was 296 nm.

CHAPTER 5: DISCUSSION

5.1 Mechanism of diamond etch pit growth

Angus and Dyble (1975) proposed a model illustrating that diamond etch pits favour a triangular shape due to the preferential removal of two-bonded carbon atoms over three- and four-bonded atoms on the [111] surface, and furthermore that negative trigons are more energetically favourable than positive trigons because the formation of positive trigons requires removal of three-bonded carbon atoms (Angus and Dyble, 1975). The results of this study show that at the experimental conditions, there is enough energy to remove three-bonded carbon atoms and form positive trigons.

When one carbon atom is successfully removed, a "kink site" develops. In Angus and Dyble's (1975) model, atoms are removed in a "step" along the edge of the trigon moving away from the kink site in both directions. This process, called the kink mechanism, may occur as a single-kink or multiple-kink mechanism, depending on how many new kink sites are being formed (Angus and Dyble, 1975). When the time required to form a new kink site is much longer than the time required for a kink to propagate along the step, atoms will be removed by the single-kink mechanism (Angus and Dyble, 1975). When the time required to form a new kink site is much shorter than the time required for a kink to propagate along the step, atoms will be removed by the multiple-kink mechanism (Angus and Dyble, 1975).

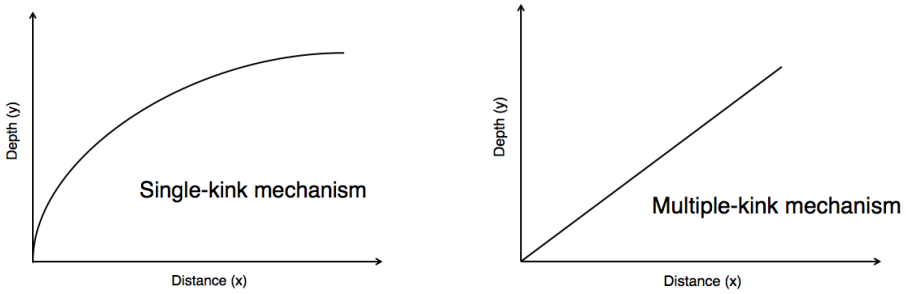

Figure 5.1. Effect of kink mechanism on trigon wall slope proposed by Angus and Dyble (1975). (a) shows that when carbon atoms are removed via the single-kink mechanism, the slope of the trigon wall will decrease as distance from the centre of the trigon increases. (b) shows that when carbon atoms are removed via the multiple-kink mechanism, the slope of the trigon wall will remain constant. After Angus and Dyble (1975).

Angus and Dyble (1975) state that when atom removal occurs via the single-kink method, the slope of the trigon wall will decrease as distance from the center of the trigon increases. According to the wall slope classifications used in this study, the single-kink mechanism would produce Y-shaped trigons. When atom removal occurs via the multiple-kink mechanism, the slope of the trigon will remain constant as distance from the center of the trigon increases (Angus and Dyble, 1975). Using the classifications in this study, the multiple-kink mechanism would produce V-shaped trigons. Figure 5.1 shows how trigon wall slope differs between the two mechanisms.

The results of this study were that in Na_2CO_3 melt, diamonds developed Y-shaped trigons. In Na_2CO_3-NaCl melt, diamonds developed Y-, V-, and U-shaped trigons. In Na_2CO_3-NaF melt, diamonds developed only Y-shaped trigons. Comparison to Angus and Dyble's (1975) model indicates that in Na_2CO_3 and Na_2CO_3-NaF melt the single-kink mechanism was dominant, while in Na_2CO_3-NaCl melt both the single- and multiple-kink mechanism were active. Since the multiple-kink method requires that the time required to form a new kink site be less than the time required for a kink to propagate along a step,

there must be some mechanism occurring in the Na_2CO_3-NaCl melt that makes it easier to form new kink sites.

Etch pits begin to form at defect sites on the diamond surface, a process called selective etching (Khokhryakov et al, 2006). Trigon morphology may be related to the type of defect at the trigon nucleation point. Results of selective etching experiments have suggested that point-bottomed etch pits form from dislocations, and that flat-bottomed trigons form from shallow surface defects such as impurity agglomerations or microcracks (Khokhryakov et al, 2006). The results of this study show that in some compositions, different types of defects do not always produce different trigon morphologies, and some melt compositions better expose defect type. We assume that all three diamonds used in this study have similar defect populations. In Na_2CO_3 melt, all trigons were flat-bottomed; in Na_2CO_3-NaCl melt, trigons were flat-, point-, and round-bottomed; and in Na_2CO_3-NaF melt, trigons were flat- and point-bottomed. The difference in trigon morphology with melt composition indicates that in Na_2CO_3 melt trigon morphology is not controlled by defect type, whereas in Na_2CO_3-NaCl and Na_2CO_3-NaF melt, the defect type may control the trigon morphology.

In the case of flat-bottomed trigons, once the vertical resorption of the entire [111] faces reaches the depth of the surface defect, the flat-bottomed trigons will disappear (Khokhryakov et al, 2006). The erasure of flat-bottomed trigons by vertical resorption was observed in this study's experiments, as most of the flat-bottomed trigons on EK-1 that were present after run 1 disappeared after run 2. Any trigon that was less than 439 nm deep on EK-1 after run 1 was no longer there after run 2. This indicates that the

controlling factor for flat-bottomed trigon depth is the depth of the surface defect around which they nucleate.

There are several opposing ideas on the mechanism for trigon morphological development. Arima and Kozai (2008) postulated that trigons begin as small flat-bottomed trigons and with progressive dissolution become larger point-bottomed trigons. Khokhyrakov and Palyanov (2006), on the other hand, showed initially small point-bottomed trigons developing into larger flat-bottomed trigons with progressive dissolution. Zhang et al (2015) also suggested that trigons begin as small point-bottomed trigons and develop into larger flat-bottomed trigons. Fedortchouk (2015) demonstrated the effect of fluid composition, suggested that in H_2O fluid, the time required to form a new kink site is so much longer than the time required for a kink to propagate around the perimeter of the pit that three-bonded carbon atoms on the bottom on the pit are not easily removed and flat-bottomed trigons develop (Figure 5.1). In contrast, in CO_2 fluid, the time required to form a new kink site is close enough to the time required for kink propagation around the pit perimeter that atoms on the bottom of the pit may be removed easily enough for point-bottomed trigons to form (Fedortchouk, 2015).

My results did not confirm whether trigons progress from small, point-bottomed trigons to large flat-bottomed trigons. All trigons retained the same morphology between run 1 and run 2. However, in many cases for flat-bottomed trigons, the diameter of the bottom of the trigon grew between run 1 and run 2 with virtually no change in depth. This could be a sign that the initial surface defect that the trigon nucleated on was no longer present at the depth of the bottom of the trigon, and that atoms were only being

removed from the walls. This is in agreement with postulations from Khokhryakov et al. (2006).

5.2 Effect of halogens on diamond resorption

Rudenko et al. (1967) proposed that diamond dissolution occurs when volatile molecules such as H_2O or CO_2 attach to carbon atoms on the diamond surface, forming various HCO complexes that break the C-C bonds to liberate carbon atoms from the diamond structure. On the diamond surface, the carbon atoms that are not bound to the layer below have one free valence electron perpendicular to the diamond surface (Rudenko et al, 1967). The free valence electrons are saturated with monovalent molecules, the most probable being OH^-, which could also easily be replaced by Cl^- or F^- (Rudenko et al, 1967). Figure 5.2 shows the mechanism of diamond oxidation when Cl and CO_2 are present postulated by Rudenko et al. (1967).

Sonin et al. (2008) showed that NaCl and NaF halogenide melts were capable of etching diamonds at 3 GPa and 1300-1350ºC, however chloride contents in the Udachnaya-East kimberlite pipe are not high enough to be the sole diamond etchtant. Sonin et al. (2009) conducted dissolution experiments with silicate-NaCl and silicate-NaF melts at 3 GPa and 1350ºC and found that negative trigons developed similar to those observed on natural kimberlitic diamonds. As diamond dissolution rate is much higher in hydrous fluid than in “dry” silicate fluid, Sonin et al. (2009) proposed that a silicate-halogenide fluid would be better able to preserve diamonds during transport to the surface, while still causing diamond dissolution features to develop.

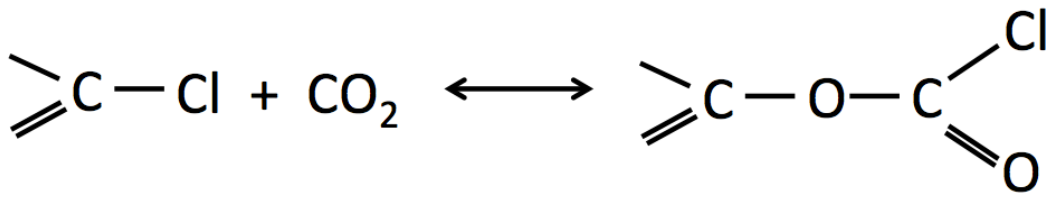

Figure 5.2. Cl-C-O complex on the diamond surface during diamond oxidation by CO_2. Rudenko et al. (1967) propose that the formation of such complexes makes it easier to remove carbon atoms from the diamond lattice. After Rudenko et al. (1967).

My results show that the presence of halogens affects the character of diamond resorption at atmospheric pressure. In Na_2CO_3 melt, diamond edges became rounded and the [111] face was covered with large flat-bottomed positive trigons. The maximum amount of vertical resorption (439 nm) occurred in this melt. In Na_2CO_3-NaCl melt, diamond edges did not become rounded, the [111] face was covered with numerous flat-, point-, and round-bottom positive trigons with that ranged in size from very small to large, and the smallest amount of vertical resorption (140 nm) occurred. In addition, a large circular feature developed on the center of two opposing faces. In Na_2CO_3-NaF melt, very little rounding of diamond edges occurred and the [111] face was covered in medium to large flat- and point-bottomed trigons. The amount of vertical resorption was intermediate (296 nm) compared to the other diamonds and melt compositions. In general, the presence of halogens in the melt supressed vertical resorption and diamonds in carbonate-halogen melts developed flat-, point- and round-bottomed trigons, whereas diamond in pure carbonate melt developed only flat-bottomed trigons.

One way that halogen presence in the etching fluid may affect resorption is by decreasing the viscosity of the melt, allowing for faster diffusion. If halogen presence in the melt increased diffusion of carbon into the melt, the overall dissolution rate would be expected to increase. The dissolution rates in Na_2CO_3, Na_2CO_3-NaCl, and Na_2CO_3-NaF

melts measured in this study were 0.011 mg/(hr*mm^2), 0.014 mg/(hr*mm^2), and 0.021 mg/(hr*mm^2) respectively. These rates indicate that the dissolution rate increased when halogens were present.

I suggest another mechanism, aside from altering the viscosity, that halogen presence in the etching fluid may affect resorption. In Figure 5.2, the complex that forms on the diamond surface when Cl fills the free valence of carbon atoms on the surface has Cl and O on one end. Since Cl and O are the third- and second-most electronegative elements, that end of the complex would be very electronegative and would tend to attract electrons. Electrons from the end of the complex, where carbon is bound to the surface of the diamond, would be pulled towards the other end of the complex, effectively weakening the bonds that carbon holds with other carbons on the diamond surface. This process is called the inductive effect. Weakening the C-C bonds between carbon atoms on the surface of the diamond would make it easier to remove them.

Weakening of C-C bonds on the diamond surface may encourage the formation of new kink sites during trigon etching, explaining why the multiple-kink mechanism was more active in Na_2CO_3-NaCl melt than in Na_2CO_3 melt. However, if both Cl and F are extremely electronegative, the multiple-kink mechanism would be expected to be active during etching in Na_2CO_3-NaF melt, which was not the case.

5.3 Diamond dissolution conditions in Snap Lake kimberlite

Li et al. (2015) examined 251 microdiamonds from the Snap Lake kimberlite. Diamonds had both negative and positive trigons, indicating two phases of resorption at depth and at the surface (Li et al, 2015). The negative trigons had truncated corners,

similar to the truncated corners that developed on the large negative trigon initially present on EK-2 in Na_2CO_3-NaCl melt. The positive trigons on the Snap Lake diamonds showed a range of morphologies, including flat-, point-, and round-bottomed, and were believed to have formed at temperatures < 1000ºC based on comparison with experimental results (Li et al, 2015). Li et al. (2015) proposed that the different morphologies of the positive trigons were a product of three different trigon evolution trends, based on the observation that each diamond from the Snap Lake kimberlite tended to show only one type of positive trigon morphology. According to Li et al. (2015), the diamonds were exposed to different resorption conditions that produced different positive trigon morphologies, and under the same resorption conditions, only one type of positive trigon morphology should be present.

The results of this study show that it is possible to create more than one type of positive trigon morphology on the same diamond face in the same resorption conditions. In the case of EK-2 in Na_2CO_3-NaCl, flat-, point-, and round-bottom trigons of varying sizes were produced on the same face under the same conditions. Similarly, EK-3 in Na_2CO_3-NaF developed flat- and point-bottomed trigons in the same conditions. These observations suggest that although differences in melt composition influence positive trigon morphology, differences in trigon morphology do not always indicate a difference in resorption conditions between diamonds. The different positive trigon morphologies observed on EK-2 and EK-3 could be a result of different types of defects on the diamond surface.

The diamonds from the Snap Lake kimberlite contained positive trigons < 4 μm in diameter and < 350 nm in depth, with a range of flat-, point-, and round-bottomed

morphologies (Li et al, 2015). The only experiment carried out in this study that produced positive trigons with all three types of morphologies as well as comparable diameters and depths was EK-2 in Na_2CO_3-NaCl melt. Although group 1 trigons on EK-2 were >15 μm in diameter and much larger than positive trigons on Snap Lake diamonds, group 2 trigons on EK-2 were < 6 μm in diameter after run 1 and < 10 μm in diameter after run 2. These results indicate that the trigons on diamonds from Snap Lake kimberlite could have been exposed to a carbonate-chlorine melt at atmospheric pressure if the time exposed to the fluid was an hour or less.

CHAPTER 6: CONCLUSIONS

Diamonds develop positive trigons in Na_2CO_3, Na_2CO_3-NaCl, and Na_2CO_3-NaF melts at 950ºC and 0.1 MPa. Halogen presence in the melt affects trigon morphology. In Na_2CO_3 melt, trigons are flat-bottomed with Y-shaped walls. In Na_2CO_3-NaCl melt, trigons are flat-, point-, and round-bottomed with Y-, V-, and U-shaped walls. In Na_2CO_3-NaF melts, trigons are flat- and point-bottomed with Y-shaped walls. According to Angus and Dyble's (1975) model, trigon wall slope may be related to the mechanism of carbon atom removal during dissolution. The presence of trigons with only Y-shaped walls on EK-1 and EK-3 exposed to Na_2CO_3 and Na_2CO_3-NaF melts respectively indicates that the single-kink mechanism was active during dissolution; in contrast, the presence of trigons with Y- and V- shaped walls on EK-2 exposed to Na_2CO_3-NaCl indicates that both the single- and multiple-kink mechanism were active during dissolution.

Diamonds are oxidized during dissolution by the formation of HCO complexes on the diamond surface, which make it easier to remove carbon atoms from the diamond lattice. The presence of halogens in the melt may alter these HCO complexes in such a way that the strong electronegativity of Cl or F destabilizes the bonds between carbon atoms in the diamond lattice and makes removal even easier. If this were the case, the multiple-kink mechanism of atom removal would be favoured and trigons would tend to have V-shaped wall slopes. V-shaped trigon wall slopes observed on EK-2 in Na_2CO_3-NaCl melt support this idea.

The results of this study could not confirm whether trigons evolve from point- to flat-bottomed during development or vice versa, as all trigons maintained the same morphology between run 1 and run 2. However, the nature of flat-bottomed trigon growth, where trigon depth seems to hit a certain depth and remain fixed while diameter continues to increase, indicates that flat-bottomed trigon depth may be controlled by the depth of the surface defect around which it nucleated.

Comparison of experimental dissolution features with dissolution features on diamond from the Snap Lake kimberlites indicates that the diamonds may have been exposed to carbonate-chlorine fluid at atmospheric pressure and 950ºC for less than an hour. If the Snap Lake kimberlite magma contained chlorine as a volatile, alteration post-emplacement may explain why the kimberlite is not chlorine-rich.

REFERENCES

Angus, J.C. and Dyble, T.J. 1975. Etching models for a {111} diamond surface: calculation of trigon slopes. Surface Science, 50, 157–177.

Arima, M. and Kozai, Y. 2008. Diamond dissolution rates in kimberlitic melts at 1300–1500ºC in the graphite stability field. Eur. J. Mineral. 20, 357–364.

Brooker, R.A., Sparks, R.S.J., Kavanagh, J.L., and Field, M. 2011. The volatile content of hypabyssal kimberlite magmas: some constraints from experiments on natural rock compositions. Bull. Volcanol. 73, 959–981.

De Beers Canada Inc. Kimberlite Petrology Unit. n.d. Internal Report. pp. 17–111.

Dove, P.M. and Platt, F.M. 1995. Compatible real-time rates of mineral dissolution by Atomic Force Microscopy (AFM). Chemical Geology, 127, 331–338.

Eckstrand, O.R., Sinclair, W.D., and Thorpe, R.I. 1995. Geology of Canadian mineral deposit types. No. 8, Geological Survey of Canada.

Fedortchouk, Y., Canil, D., and Semenets, E. 2007. Mechanisms of diamond oxidation and their bearing on the fluid composition in kimberlite magmas. American Mineralogist, 92, 1200–1212.

Fedourtchouk, Y., Canil D. 2009. Diamond oxidation at atmospheric pressure: development of surface features and the effect of oxygen fugacity. Eur. J. Mineral. 21: 623–635.

Fedortchouk, Y. and Zhang, Z. 2011. Diamond resorption: link to metasomatic events in the mantle or record of magmatic fluid in kimberlitic magma? The Canadian Mineralogist, 49, 707–719.

Fedortchouk, Y. 2015. Diamond resorption features as a new methods for examining conditions of kimberlite emplacement. Contrib. Mineral. Pertrol. 170, 36.

Gernon, T.M., Field, M., and Sparks, R.S.J. 2012. Geology of the Snap Lake kimberlite intrusion, Northwest Territories, Canada: field observations and their interpretation. Journal of the Geological Society, London. 169, 1–16.

Gurney J.J., Hildebrand, P.R., Carlson, J.A., Fedortchouk, Y., and Dyck, D.R. 2004. The morphological characterstics of diamonds from the Ekati property, Northwest Territories, Canada. Lithos, 77, 21–38.

Howland, R. and Benatar, L. 1993–2000. A Practical Guide to Scanning Probe Microscopy. Thermomicroscopes.

Kamenetsky, V.S., Maas, R., Kamenetsky, M.B., Paton, C., Phillips, D., Golovin, A.V., and Gornova, M.A. 2009. Chlorine from the mantle: Magmatic halides in the Udachnaya-East kimberlite, Siberia. Earth and Planetary Science Letters, 285, 96–104.

Khokhryakov, A.F., Palyanov, Y.N., and Sobolev, N.V. 2001. Evolution of crystal morphology of natural diamond in dissolution processes: Experimental data. Doklady Earth Sciences, 381, 884–888.

Khokhryakov, A.F., Palyanov, Y.N., and Sovolev, N.V. 2002. Crystal morphology as an indicator of redox conditions of natural diamond dissolution at the mantle PT parameters. Doklady Earth Sciences, 385, 534–537.

Khokhryakov, A.F. and Palyanov, Y.N. 2006. Revealing of dislocations in diamond crystals by the selective etching method. Journal of Crystal Growth, 293, 469–474.

Khokhryakov, A.F. and Palyanov, Y.N. 2010. Influence of the fluid composition on diamond dissolution forms in carbonate melts. American Mineralogist, 95, 1508–1514.

Kozai, Y. and Arima, M. 2005. Experimental study on diamond dissolution in kimberlitic and lamproitic melts at 1300–1420ºC GPa with controlled oxygen partial pressure. American Mineralogist, 90, 1759–1766.

Li, Z., Fedortchouk, Y., Chinn, I., and Fulop, A. 2015. Micromorphology and resorption of diamonds from Snap Lake and Ekati Mine kimberlites (Canada) as an indicator of fluid and emplacement history. Presented as a poster at GacMac 2015.

Mitchell, R.H. 1986. Kimberlites: Mineralogy, Geochemistry, and Petrology. Plenum Press, New York and London.

Orlov, Y.L. 1973. Mineralogy of diamond. Izd. Acad. Of Sci. of the USSR, Moscow (In Russian).

Robinson, D.N. 1979. Surface Textures and Other Features of Diamonds. Ph.D. thesis, 206 pp., University of Cape Town at Cape Town, December.

Rudenko, A.P., Kulakova, I.I., and Balandin, A.A. 1967. Structural and energetic factors in the catalytic oxidation of diamond. Vestnik Moskovskogo Universiteta, 22, 105–117.

Sonin, V.M., Zhimulev, E.I., Chepurov, A.I., and Fedorov, I.I. 2008. Diamond stability in NaCl and NaF melts at high pressure. Doklady Earth Sciences, 420, 641–643.

Sonin, V.M., Zhimulev, E.I., Chepurov, A.I., and Pokhilenko, N.P. 2009. Diamond stability in silicate-halogenide melts at high pressure. Doklady Earth Sciences, 425A, 441–443.

Tappert, R. and Tappert, M.C. 2011. Diamonds in Nature: A Guide to Rough Diamonds. Springer-Verlag, Berlin Heidelberg.

Veeco, 2010. Multimode 8 with ScanAsyst Instruction Manual. Veeco Instruments, Inc.

Wentorf R.H. 1965. Diamond synthesis. Advances in Chemical Physics. 9, 365–404.

Yamaoka, S., Kanda, H. and Setaka, N. 1980. Etching of diamond octahedrons at high temperatures and pressure with controlled oxygen partial pressure. Journal of Materials Science, 15: 332–336.

Zhang, Z., Fedortchouk, Y., and Hanley, J. 2015. Evolution of diamond resorption in a silicic aqueous melt at 1-3 GPa: application to kimberlite emplacement and mantle metasomatism. LITHOS.